Lithos 318–319 (2018) 283–298

Contents lists available at ScienceDirect

Lithos

journal homepage: www.elsevier.com/locate/lithos

Petrogenesis of the Early Cretaceous granitoids and its mafic enclaves in the Northern Tengchong Terrane, southern margin of the Tibetan Plateau and its tectonic implications

Jingyi Zhang [a,b], Touping Peng [a,c,*], Weiming Fan [b,c], Guochun Zhao [d], Xiaohan Dong [a,b], Jianfeng Gao [e], Bingxia Peng [a], Chao Wei [a,b], Xiaoping Xia [a], Linli Chen [a], Xirong Liang [a]

[a] State Key Laboratory of Isotope Geochemistry, Guangzhou Institute of Geochemistry, Chinese Academy of Sciences, Guangzhou 510640, China
[b] University of Chinese Academy of Sciences, Beijing 100049, China
[c] CAS Center for Excellence in Tibetan Plateau Earth Sciences, Beijing 100101, China
[d] Department of Earth Sciences, The University of Hong Kong, Hong Kong, China
[e] State Key Laboratory of Ore Deposit Geochemistry, Institute of Geochemistry, Chinese Academy of Sciences, Guiyang 550081, China

ARTICLE INFO

Article history:
Received 12 May 2018
Accepted 13 August 2018
Available online 16 August 2018

Keywords:
Early Cretaceous
Na-rich granitoids
Mafic enclave
Tengchong Terrane
Myitkyina Tethys Ocean

ABSTRACT

Cretaceous granites are widely exposed in the Tengchong Terrane that is the southern extension of the Tibetan Plateau, resulting from the evolution of the Tethys. They, therefore, play a critical role in deciphering the Tethys evolution and the growth of the Tibetan Plateau. In this paper, we present new zircon U—Pb dating and Hf isotopic results, along with whole-rock elemental and Sr—Nd isotopic data of the granitoids from the Lushui-Pianma (LP) batholith and its mafic enclaves and the strongly deformed granites from the Gaoligong shear zone in the northern Tengchong Terrane. The dating results show that both the LP granitic batholith and the strongly deformed granites in the Gaoligong shear zone formed in the Early Cretaceous of 122–110 Ma. They are composed of granodiorite, quartz monzodiorite and monzogranite with minor gabbroic enclaves. Mineralogically and geochemically, the granitoids in the LP batholith, particularly for the less evolved ones, display a metaluminous nature and an affinity to I-type granite. All the granitoids are characterized by similar rare and trace patterns and whole-rock Nd and zircon Hf isotopic compositions, indicating a common origin. The sodium-rich feature for the less evolved dioritic rocks and the predominantly negative zircon $\varepsilon_{Hf}(t)$ and whole-rock $\varepsilon_{Nd}(t)$ values for all the granitoids demonstrate that they were derived mainly from the partial melting of the Mesoproterozoic metabasic rocks (likely the basement rocks of the Gaoligong Group) in the lower crust of the Tengchong Terrane. In the case of the mafic enclaves, they share similar mineralogical assemblages and Nd—Hf isotopic compositions to its host granodiorite, indicating a cognate origin with the latter.

In combination with previous data for the granitoids in the Tengchong Terrane, our study further illustrates that the Early Cretaceous granitic rocks are dominated by metaluminous I-type granites with minor highly fractionated peraluminous I-type granites, rather than the dominant S-type granites as assumed before. The new identification of the Myitkyina Meso-Tethys ophiolitic suite in eastern Myanmar, together with regional Early Cretaceous magmatic and sedimentation patterns, indicate that these Early Cretaceous magmatic rocks were the products of the evolution of the Myitkyina Tethys Ocean, which was related to post-collisional slab breakoff.

1. Introduction

Granitic magmas are widespread in the Tibetan Plateau and its surrounding areas (Yin and Harrison, 2000; Zhu et al., 2009), particularly along the Three-River (also referred to as the Jinshajiang, Lancangjiang and Nujiang in Western China) Tethys orogenic belts. As the products of different tectono-thermal events during the formation and evolution of this Plateau, they play an important role in unraveling precisely the spatial and temporal evolution of the Tethys and their rock-forming geodynamic mechanism. However, different types of granitic rocks can be derived from different sources, such as S-, I- and A-type granites (e.g., Eby, 1992), and even the same granite type can be generated in different tectonic environments during the evolution of orogeny, including subduction, *syn*- to post-collisional and post-orogenic extensional settings (e.g., Barbarin, 1999; Chappell and White, 1992;). Providing insights into their origin and rock-forming tectonic setting is thus critical to constrain the orogenic evolution related to the granitic magmatism.

* Corresponding author at: Guangzhou Institute of Geochemistry, Chinese Academy of Sciences, P.O. Box 1131, Guangzhou 510640, China.
E-mail address: tppeng08@126.com (T. Peng).

https://doi.org/10.1016/j.lithos.2018.08.017
0024-4937/

In recent two decades, a great number of studies have been focused on the Northern Granitic Belt (NGB) along the Bangong-Nujiang Tethys tectonic zone within the Tibetan Plateau. This granitic belt is dominated by peraluminous S-type granites, which is different from the overwhelming I-type granites of the Gangdese batholith in the Southern Lhasa (Harris et al., 1990; Kapp et al., 2005). Although the rock-forming geodynamic setting and mechanism remains debated, these studies have provided an important constraint on the precisely spatial and temporal evolution of the Bangong-Nujiang Tethys Ocean within the Tibetan Plateau (e.g., Li et al., 2014b; Sui et al., 2013; Zhu et al., 2009; Zhu et al., 2011 and references therein). As the southern extension of the NGB in the Lhasa Terrane, the Mesozoic granitic rocks in the Tengchong Terrane, Western Yunnan has attracted little attention (e.g., Fang et al., 2018; Xu et al., 2012; Zhu et al., 2015, 2017b). Moreover, most researchers have exclusively ascribed the generation of these Early Cretaceous granitoids to the products of the Lushui-Luxi-Ruili Tethys Ocean to the east of the Tengchong Terrane (e.g., Fang et al., 2018; Xu et al., 2012; Zhu et al., 2015, 2017b). Nonetheless, the new identification of the Myitkyina Tethys ophiolitic suite of the Eastern Myanmar comparable to those along the Bangonghu-Nujiang belt within the Tibetan Plateau (Liu et al., 2016a; Yang et al., 2012) likely indicate that the geodynamic setting and mechanism responsible for the generation of the Mesozoic granitic magmatism, especially for the Early Cretaceous granitoids in the Tengchong Terrane, needs to be reassessed. For example, recent studies have demonstrated that some Early Cretaceous granitic rocks in the southern Tengchong Terrane display an affinity to metaluminous I-type granites (Fang et al., 2018; Zhu et al., 2015, 2017b), rather than peraluminous S-type granites as assumed previously (Xu et al., 2012). Furthermore, the new finding of some coeval mafic enclaves hosted in the Menglian and Xiaotang granitic batholiths of the southern Tengchong Terrane reflect some contributions from the mantle-derived magma to the host granitoids (Zhu et al., 2017b), likely the heat or materials or both, although the Early Cretaceous mafic magmatic rocks have not been exposed in the region. In the case of the granitic batholith in the Lushui-Fugong region of the northern Tengchong Terrane (Fig. 1a), whether their source region is different from the southern ones remains unclear. Our finding of mafic enclaves hosted in the LP granitic batholith can give some critical insights into this issue.

An alternative point is that, except for the undeformed granitic plutons, some deformed granitic gneisses in the metamorphic complex (generally termed as Gaoligong Group in Chinese literature) to the west of the Gaoligong shear zone (GSZ) were confirmed to be Cretaceous (Xie et al., 2016 and references therein). This indicates a more widespread development of the Early Cretaceous granitic rocks in the Tengchong Terrane than proposed before (Fig. 2). Furthermore, some Early Paleozoic granitic rocks have also been recognized within the GSZ that was considered previously as the Precambrian basement rocks (Xie et al., 2016; YNBGMR, 1990). Whether the shear zone also comprises much more Early Cretaceous granitic rocks is still unknown.

In this paper, we present new zircon LA-ICP-MS U—Pb dating and Hf isotopic data, and whole-rock geochemical and Sr—Nd isotopic results for the Early Cretaceous granitoids from the LP batholith and strongly deformed granites from the GSZ in the northern Tengchong Terrane of SW China (Figs. 1 and 2). Our results, coupled with regional data, are used to shed lights on: (1) the spatial and temporal pattern of Early Cretaceous magmatism in the Tengchong Terrane, (2) the origin and genesis of the mafic enclaves and its host granitoids, and (3) their rock-forming geodynamic regime and mechanism.

2. Geological background and sampling

The Tengchong Terrane together with the Baoshan Terrane in the southwestern Yunnan is considered to be the northern continuation of the Sibumasu Block (e.g., Metcalfe, 2013), which extends northwards into the Tibetan Plateau (Fig. 1a). It is separated from the Baoshan Terrane to the east by the Bangong-Nujiang-Longlin-Ruili Fault (suture zone?) and from the West Burma Terrane to the west by the Sagaing Fault (Fig. 1b; Li et al., 2014a; Xu et al., 2012; Yang et al., 2012). The widely-distributed metamorphic complexes in the Tengchong Terrane, generally termed as the Neo-Paleoproterozoic Gaoligong Group, are composed mainly of leptynite, schist, silicolite, marble, and slate, which have experienced greenschist–amphibolite facies metamorphism (Li et al., 2012b; YNBGMR, 1990; Zhao et al., 2017a). The Carboniferous–Lower Permian sequences are extensive and consist mainly of glacial-marine diamictite, sandstone, and limestone (Fig. 1b; YNBGMR, 1990). Some Silurian–Devonian and Lower Cretaceous strata comprising sandstone and mudstone are exposed sporadically in the central–eastern part of the Tengchong Terrane. It was intruded by abundant Mesozoic–early Cenozoic undeformed granitic plutons or batholiths and minor dykes (Xie et al., 2016; Xu et al., 2012; YNBGMR, 1990; Zhu et al., 2017b), and covered by voluminous Cenozoic volcanic rocks (YNBGMR, 1990; Zhu et al., 1983).

The Early Cretaceous granitoid intrusions were widely cropped out and formed as a belt mostly in the eastern Tengchong Terrane close to the GSZ (Fig. 2). This granitic belt extends over a length of 400 km and is bounded by the Lushui – Luxi – Ruili Fault (LLRF) to the east and the Gudong – Tengchong – Dayingjiang Fault (GTDF) to the west (Fig. 2; Xie et al., 2016). They are composed of three large granitic batholiths, from north to south, including the Fugong – Pianma, Menglian and Xiaotang batholiths (Fig. 2; e.g., Xie et al., 2016; Xu et al., 2012; YNBGMR, 1990). The LP batholith is located in the north of the granitic belt and intruded into the early termed Gaoligong Group metamorphic rocks (Figs. 2 and 3). The main rock units exposed in this area vary from granodiorite, quartz monzodiorite to monzogranite (Fig. 4a, b) with minor mafic enclaves (Fig. 4c). In addition, abundant granitic gneisses, migmatites and leucogranites cropped out within the GSZ (Fig. 4d, e), which were previously regarded as the basement rocks of the Gaoligong Group (e.g., YNBGMR, 1990). However, recently precise dating of zircon U—Pb revealed that some of the protoliths of granitic gneisses, migmatites and leucogranites of the Gaoligong Group within the terrane were generated during the Mesozoic times (e.g., Ma et al., 2013; Song et al., 2007; Xu et al., 2012) and minor strongly deformed granitic rocks within the GSZ were emplaced in the Paleozoic era (Fig. 2; Xie et al., 2016 and references therein).

In this study, four undeformed granitoid samples from the LP batholith and three strongly deformed granitic rocks from the GSZ were collected for LA-ICP-MS zircon U—Pb dating (Fig. 3). The samples for zircon dating including 13TB-43 (N25°57.215, E98°44.451), 13TB-47 (N25°57.045, E98°44.713), 13TB-44 (N25°57.206, E98°44.481) and 13TB-51 (N25°57.923, E98°46.821) were from the center to the eastern part of the LP batholith, meanwhile other three samples (13TB-45, 13TB-48 and 13TB-49) were collected for chemical analyses. Besides, the sample 13TB-50, as an enclave, was collected together with its host rock 13TB-51 at the same GPS locality. All studied samples have not undergone any metamorphism. The LP batholith consists mainly of granodiorite and quartz monzodiorite with minor monzogranite (Fig. 5), which are coarse-grained and massive. The granodiorites are composed of K-feldspar (18–20 vol%), plagioclase (~62–65 vol%), quartz (~15–18 vol%), amphibole (~8 vol%) and biotite (~2 vol%), with minor zircon, apatite, titanite and iron oxides. The quartz monzodiorites comprise of K-feldspar (~10–20 vol%), plagioclase (~50–60 vol%), quartz (~22–28 vol%), amphibole (~5 vol%) and biotite (~5–8 vol%). Accessory minerals include zircon, apatite, titanite and iron-oxides.

The mafic enclave is rare in the LP batholith compared to the Menglian and Xiaotang batholiths in the central-southern Tengchong Terrane (Zhu et al., 2017b). The LP mafic enclave is oval in shape and a medium- to fine-grained gabbroic enclave. Its mineral

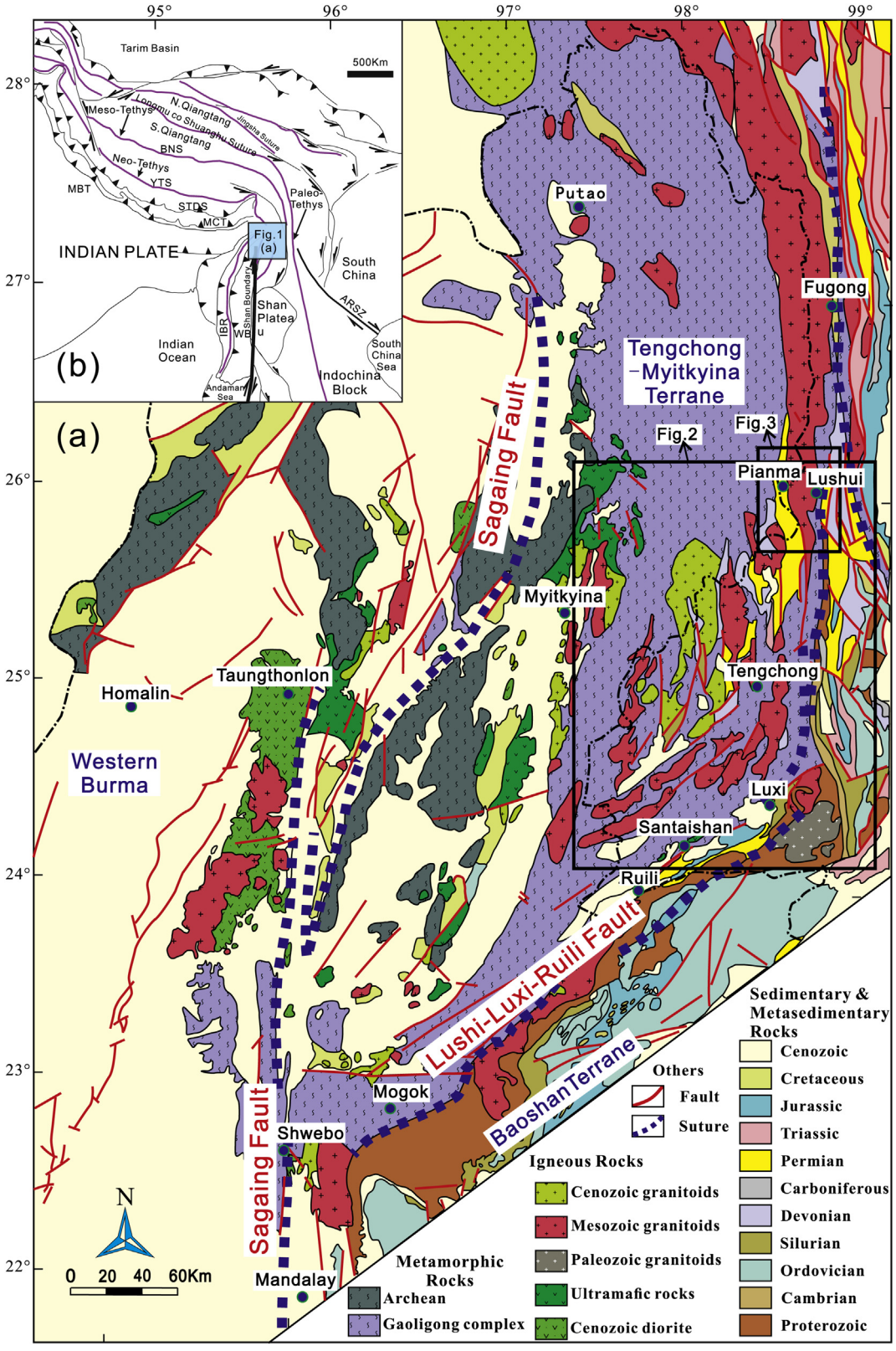

Fig. 1. Simplified geological map showing the tectonic framework of the Tengchong Terrane (modified from Geological Map of Southeastern Asia at 1:1,500,000 scale). The insert shows the relationship between the Tengchong Terrane and the Tibetan Plateau.

assemblage comprises plagioclase (~40 vol%), hornblende (~30 vol%), biotite (~20 vol%) and quartz (~5 vol%), with accessory magnetite, apatite, and zircon. Some of felsic minerals contain some inclusions, especially for the core-grained ones, showing a pervasive poikilitic texture.

In addition, three strongly deformed samples 13TB-52 (N25°58.580, E98°47.650), 13TB-53 (N25°58.919, E98°47.981) and 13TB-54 (N25°58.921, E98°48.413) for zircon dating were collected from the GSZ to the east of the LP batholith. These granites have banded structure with distinctly oriented minerals. They are monzogranitic and contain

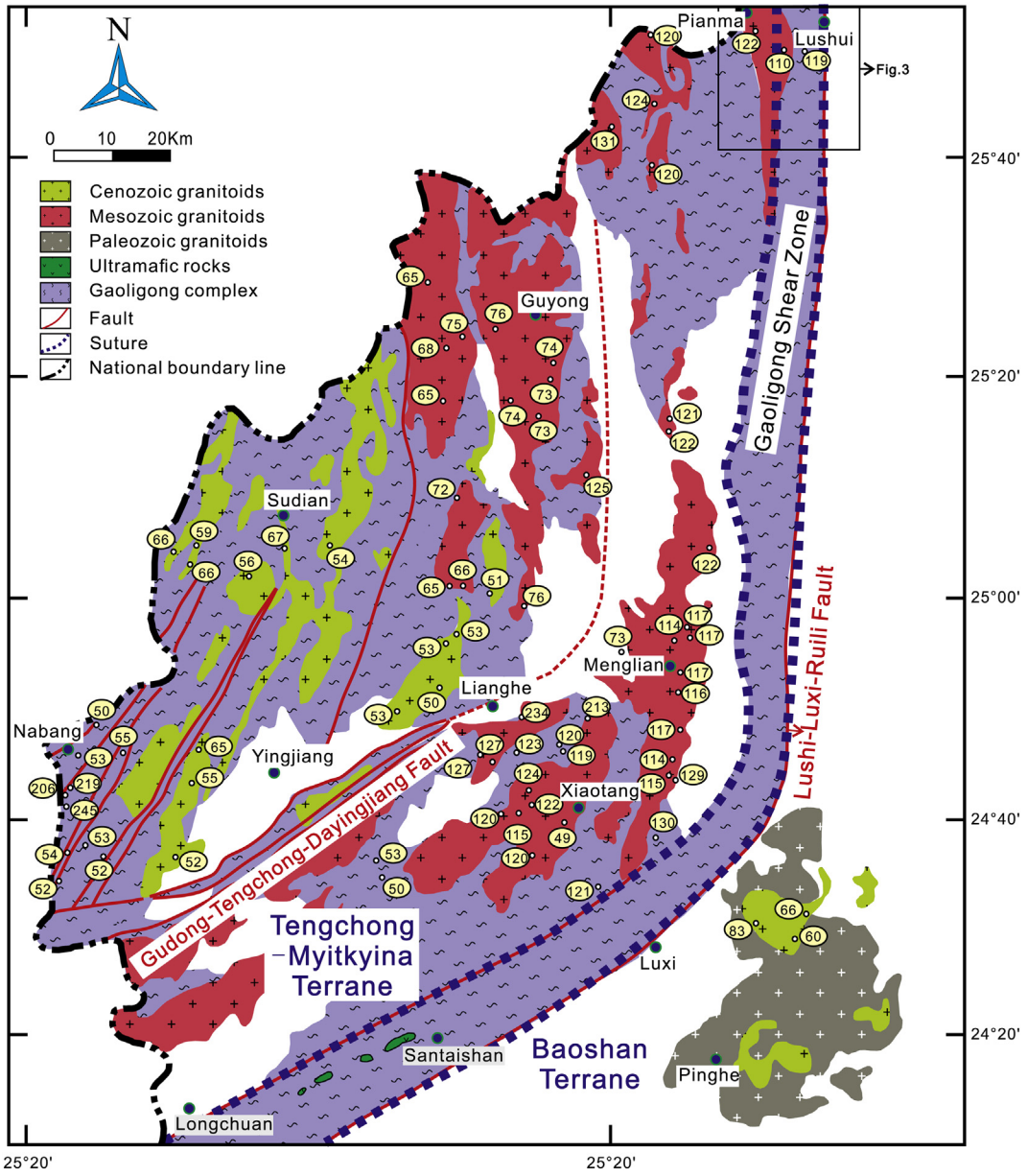

Fig. 2. Simplified geological map (after Xie et al. (2016)) showing the spatial and temporal distribution of the magmatic rocks in the Tengchong Terrane. The figures such as 110 in the circles representing the zircon U—Pb age, are from Zhu et al. (2017a, 2017b), Fang et al. (2018), Xie et al. (2016) and references therein and this study.

K-feldspar (~28–35 vol%), plagioclase (~26–38 vol%) and quartz (~33–40 vol%) with varying amounts of biotites (~3–5 vol%).

3. Analytical methods

3.1. Zircon U—Pb dating

Zircons for LA- ICP-MS U—Pb dating were separated by conventional heavy liquid and magnetic techniques and subsequently purified by handpicking under a binocular microscope. Individual zircon crystals were mounted in epoxy resin, polished to remove the upper half of the grains, and after that, photographed in transmitted and reflected light. Cathodoluminescence (CL) images were obtained using an EMPA-JXA-8100 scanning electron microscope at the State Key Laboratory of Isotope Geochemistry, Guangzhou Institute of Geochemistry, Chinese Academy of Sciences (SKLIG-GIGCAS), for inspecting internal structures of zircon grains and for choosing potential target sites for U—Pb and Hf isotope analyses. Zircon U—Pb age data were obtained by LA-ICP-MS at the Nanjing FocuMS Technology Co. Ltd., using Agilent 7700× coupled to a 193 nm excimer ArF laser-ablation system (GeoLas Plus). Detailed analytical procedures were laid out by Sun et al. (2017). The fractionation correction and results were calculated using ICPMSDataCal (Liu et al., 2010b). Harvard zircon 91500 was used as a calibration standard and U—Pb raw data were corrected offline using ICPMSDataCal 7.2 (Liu et al., 2010a; Liu et al., 2010b). ^{202}Hg is usually <10 cps in the gas blank. Therefore, the contribution of ^{204}Hg to ^{204}Pb is negligible and is not considered further. Common Pb was corrected according to the method proposed by Andersen, 2002. Isoplot (version 3.23) (Ludwig, 2003) was used for plotting Concordia diagrams and age spectra with the uncertainties on individual analyses reported as 1σ. Meanwhile, U—Pb ages were calculated using U decay constants of Steiger and Jäger (1977) and Isoplot Ex3 software (Ludwig, 2003), in which individual analyses came out within 1σ error (95% confidence level). The analyzed results are presented in Supplementary Table S1.

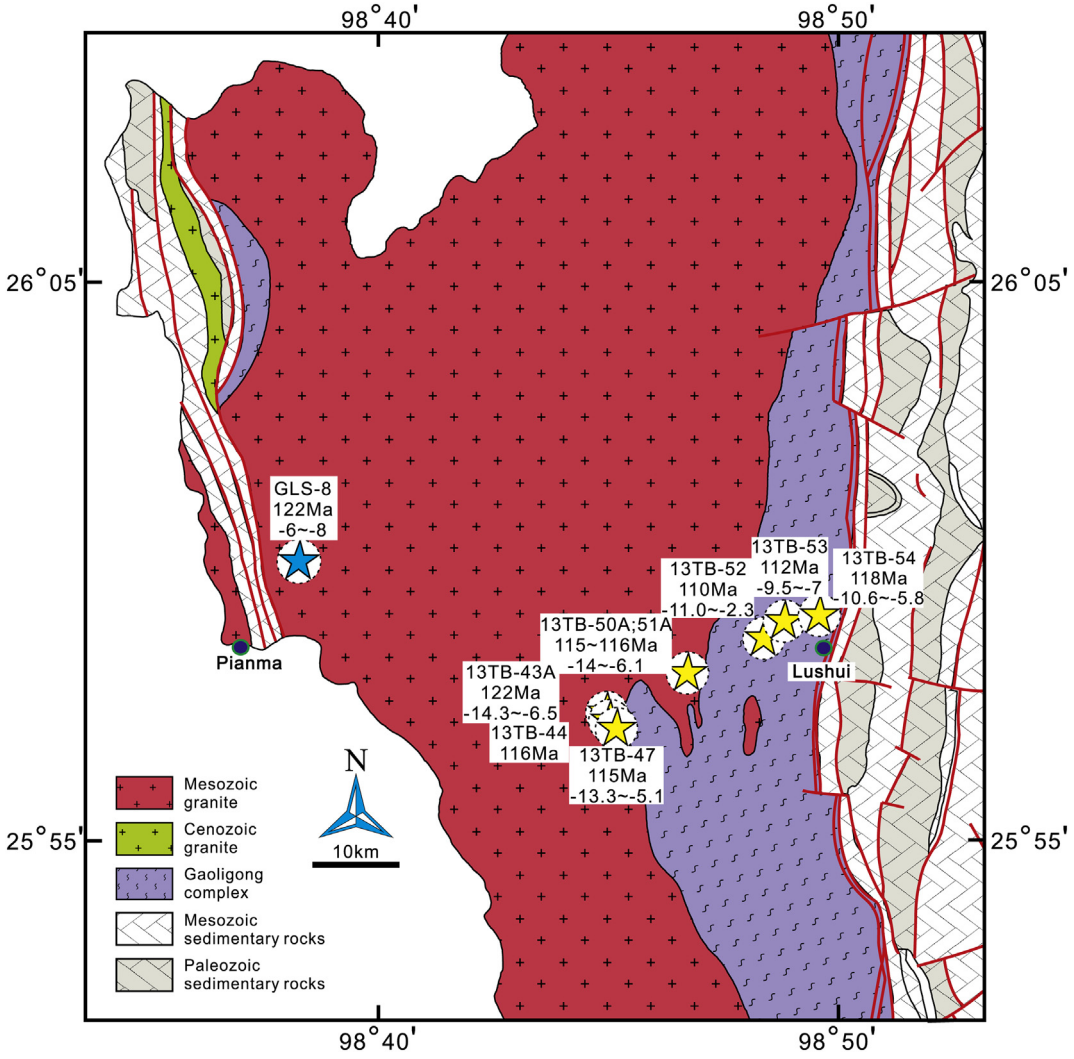

Fig. 3. Simplified geological map of the Lushui-Pianma Batholith (modified after Luxi Geological Map at 1:200,000 scale; YNBGMR, 1990), showing dating sample locations. The data of GSL-8 is from Xu et al. (2012).

3.2. Zircon Hf isotope analysis

Hf-in-zircon isotopic analysis was conducted using a Neptune Plus MC-ICP-MS, coupled to the Resonetics RESOlution M-50-LR Excimer Laser Ablation System at the SKLIG-GIGCAS. 45 μm diameter beam and 8 Hz at 80 MJ repetition rate were performed on zircon grain for acquiring Hf isotopes. The measured isotopic ratios of $^{176}Hf/^{177}Hf$ were normalized to $^{179}Hf/^{177}Hf = 0.7325$ for mass bias. The isobaric interferences of ^{176}Lu and ^{176}Yb on ^{176}Hf are monitored by the ratios of $^{176}Lu/^{175}Lu = 0.02655$ and $^{176}Yb/^{171}Yb = 0.90184$ obtained during Hf analysis on the same spot (Wu et al., 2006). Standard zircons Penglai was used as external standards and were analyzed twice before and after every 5 analyses of unknowns. Repeated Penglai measurements yielded $^{176}Hf/^{177}Hf$ ratios of 0.282905 ± 0.000012 ($n = 33$, 2σ), which is identical to the previously reported values (Li et al., 2010). The measured $^{176}Lu/^{177}Hf$ ratios and the ^{176}Lu decay constant of 1.867×10^{-11} a^{-1} (Soderlund et al., 2004) were used to calculate initial $^{176}Hf/^{177}Hf$ ratios. The $\varepsilon_{Hf}(t)$ values are calculated from chondritic values of $^{176}Hf/^{177}Hf = 0.282772$ and $^{176}Lu/^{177}Hf = 0.0332$ (BlichertToft and Albarede, 1997). The depleted mantle line is defined by present-day $^{176}Hf/^{177}Hf = 0.28325$ and $^{176}Lu/^{177}Hf = 0.0384$ (Griffin et al., 2004). A mean $^{176}Lu/^{177}Hf$ ratio of 0.015 for the average continental crust (Griffin et al., 2002) was used to calculate two-stage (crustal) model ages (T^{C}_{DM}). The Lu—Hf isotopic data are listed in Supplementary Table S2.

3.3. Whole-rock major and trace element analysis

Major element compositions of bulk rock samples were determined by wavelength X-ray fluorescence (XRF) spectrometer on fused glass disks at the SKLIG-GIGCAS, with analytical uncertainties generally better than 2%. Bulk-rock trace element analyses were performed at the Institute of Geochemistry, CAS, Guiyang, China, by inductively coupled plasma mass spectrometry (ICP-MS), with an analytical precision better than 5% for elements >10 ppm, better than 8% for those <10 ppm, and about 10% for transition metals. The detailed analytical protocol is described in (Liang et al., 2000). The obtained results are shown in Supplementary Table S3.

3.4. Whole-rock Sr—Nd isotope analysis

Sr and Nd isotopic compositions were measured using a Micromass Isoprobe multi-collector-inductively coupled plasma-mass spectrometer (MC-ICP-MS) at the SKLIG-GIGCAS. Analytical procedures for Sr and Nd isotopes are described in detail by (Liang et al., 2003). Sr and Nd isotopic fractionation was normalized to $^{86}Sr/^{88}Sr = 0.1194$ and $^{146}Nd/^{144}Nd = 0.7219$, respectively. The Sr—Nd isotopic compositions are listed in Supplementary Table S4.

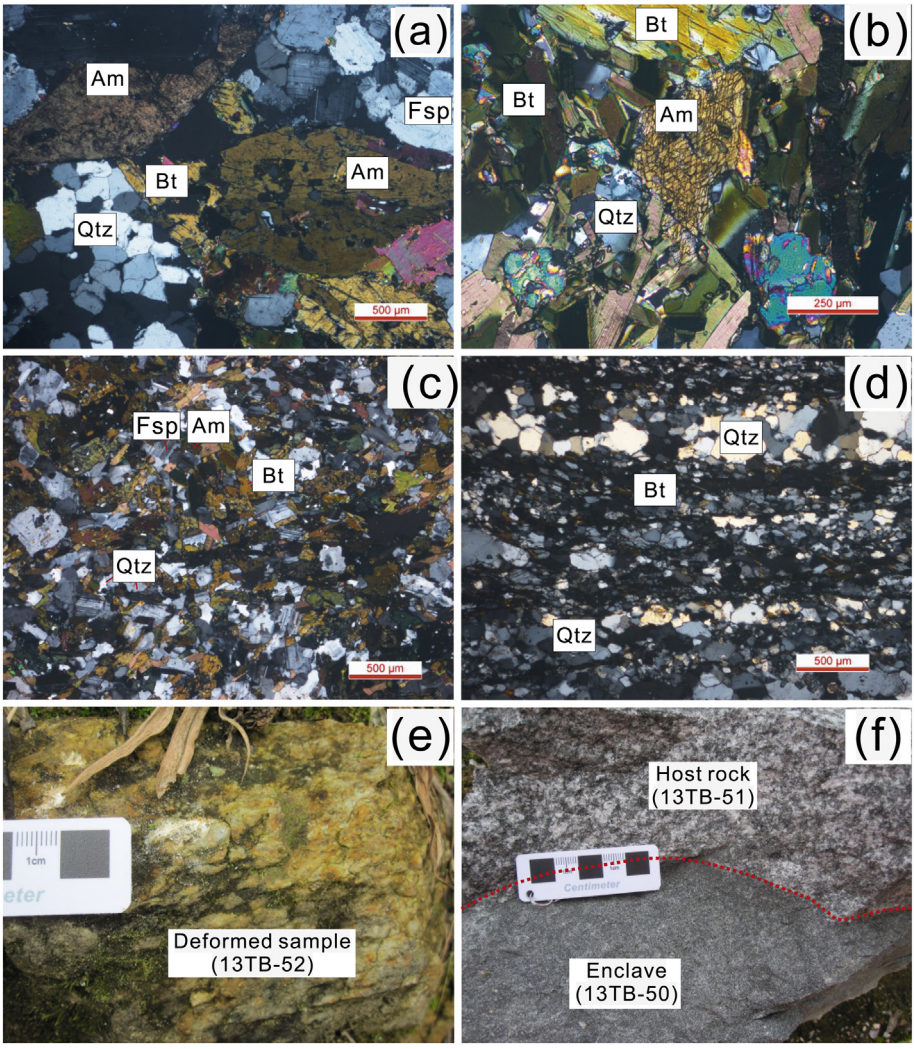

Fig. 4. Photographs of the representative samples from the Lushui-Pianma Batholith: undeformed samples (a) 13TB-43, quartz monzodiorite and (b) 13TB-51, granodiorite, (c) mafic enclave 13TB-50 hosted in sample 13TB-51, and strongly deformed granites (d) 13TB-53 and (e) 13TB-52, and (f) contact relationship between the mafic enclave and its host rock. Fsp: feldspar, Amp: amphibole, Bt: biotite, Qtz: quartz.

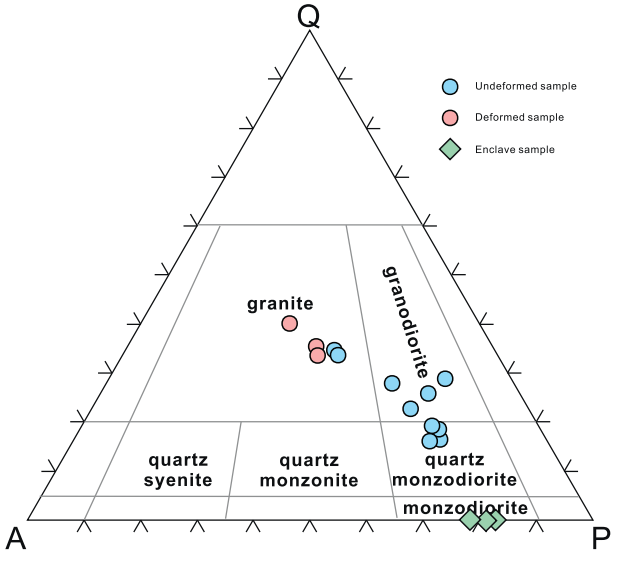

Fig. 5. Modal classification of samples from the Lushui-Pianma Batholith (after Le Maitre, 2002).

4. Results

4.1. Zircon U—Pb and Lu—Hf results

4.1.1. Mafic enclave

The zircons from the mafic enclave are subhedral and partly prismatic, and colorless to yellowish in color with the length-to-width ratios of 2:1 to 4:1. Different from its host granite (sample 13TB-51) and the deformed granitoids, most zircons show weak oscillatory zoning and are light luminescent without a core (Fig. 6). Some crystals are characterized by a small nonluminescent core surrounded by a poorly zoned, light luminescent overgrowth rim. Twenty one analyses demonstrate that, compared with the granitoids (Supplementary Table S1), most of the zircons contain relatively lower concentrations of Th (65–650 ppm) and U (50–351 ppm), but yield higher Th/U values of >1.0 with the exception of one spot having Th/U value of 0.4.

All analyzed spots of sample 13TB-50 plot below the concordia and define good discordia (Fig. 7a). The discordia calculated for all zircon fractions gives upper and lower intercept ages of 4951 ± 120 Ma and 115 ± 5 Ma, respectively. Although the upper intercept ages is meaningless, the lower intercept age is the same as the crystallization age of the host granite (116 ± 2 Ma for the sample 13TB-51) within errors (Fig. 7b), reflecting the result from the thermal effect of the host magmatic heat.

Fig. 6. Cathodoluminescence images of the representative zircons from the Lushui-Pianma Batholith. Scale bar = 100 μm; small circles are of laser U–Pb analysis and large circles of Hf isotope analysis; the numbers nearby represent U–Pb ages and $\varepsilon_{Hf}(t)$ values, respectively.

All spots with U—Pb age analyses gave zircon $\varepsilon_{Hf}(t)$ values (calculated at $t = 115$ Ma) ranging from −13.6 to −7.1 with a peak of −7.5, resembling those of the host and the deformed granitoids (Supplementary Table S2). They have the corresponding two-stage model ages of 1.08–1.50 Ga (Supplementary Table S2; Fig. 8).

4.1.2. Granite

All the zircons from both the deformed and undeformed granitoids display well-developed crystal structure. They are dominantly yellowish to brown euhedral crystals. Most grains range in length from 100 to 300 μm with length/width ratios of 1:1 to 1:3. Two different internal structures are observed. The first one is simple and core-free, with CL images showing typical magmatic oscillatory zoning towards the rim. The second one is relatively complex with the presence of resorbed, roundish, dark cores wrapped by a lighter rim (Fig. 6). These zircon grains have a wide range in U (50–5633 ppm) and Th (65–9756 ppm) concentrations. Their high Th/U ratios varying from 0.9 to 1.7, coupled with the nature of oscillatory zoning in the CL images, indicate a magmatic origin.

Most analyses of the zircons from four undeformed granitic samples (13TB-43, 13TB-44, 13TB-47 and 13TB-51) are concordant (Fig. 7b–e). They gave young weighted mean ages of 122 ± 3 Ma (MSWD = 2.0), 116 ± 3 Ma (MSWD = 1.8), 115 ± 1 Ma (MSWD = 2.3) and 116 ± 2 Ma (MSWD = 1.8), respectively. These ages can be explained as the crystallization timing of the granitic rocks. In addition, minor analyses from the zircon cores gave old ages of 2618 ± 31 Ma, 786 ± 16 Ma, 662 ± 21 Ma and 762 ± 7 Ma, such as those from the sample 13TB-43 and 13TB-47 (Supplementary Table S1), indicating an inherited origin. Similarly, three deformed granitic rocks also yielded the Early Cretaceous crystallization ages, 110 ± 1 Ma (MSWD = 2.2), 112 ± 1 Ma (MSWD = 1.6) and 118 ± 1 Ma (MSWD = 1.8) for the samples 13TB-52, 13TB-53 and 13TB-54, respectively. Likewise, some old ages were also obtained, such as 1517 ± 54 Ma from the sample 13TB-54 representing inherited zircon, and 136 ± 7 Ma and 134 ± 11 Ma from the sample 13TB-54 and 125 ± 3 Ma from the sample 13TB-52 likely representing xenocrystal zircons (Supplementary Table S1 and Fig. 7f, g and h).

All representative analyses of young age domains from the undeformed granitic rocks gave a similar zircon $\varepsilon_{Hf}(t)$ range (−14.0 to −5.1) and peak value (−7.5) to those from the strongly deformed granitic rocks (−11.0 to −2.3 and − 8.0; Fig. 8). Their corresponding two-stage model ages are 1.05–1.39 Ga and 0.89–1.23 Ga, respectively (Supplementary Table S2). Compared with those from the granitoid batholiths in the central-southern Tengchong Terrane (Zhu et al., 2017a), they mostly have lower $\varepsilon_{Hf}(t)$ values and older two-stage model ages (Fig. 8).

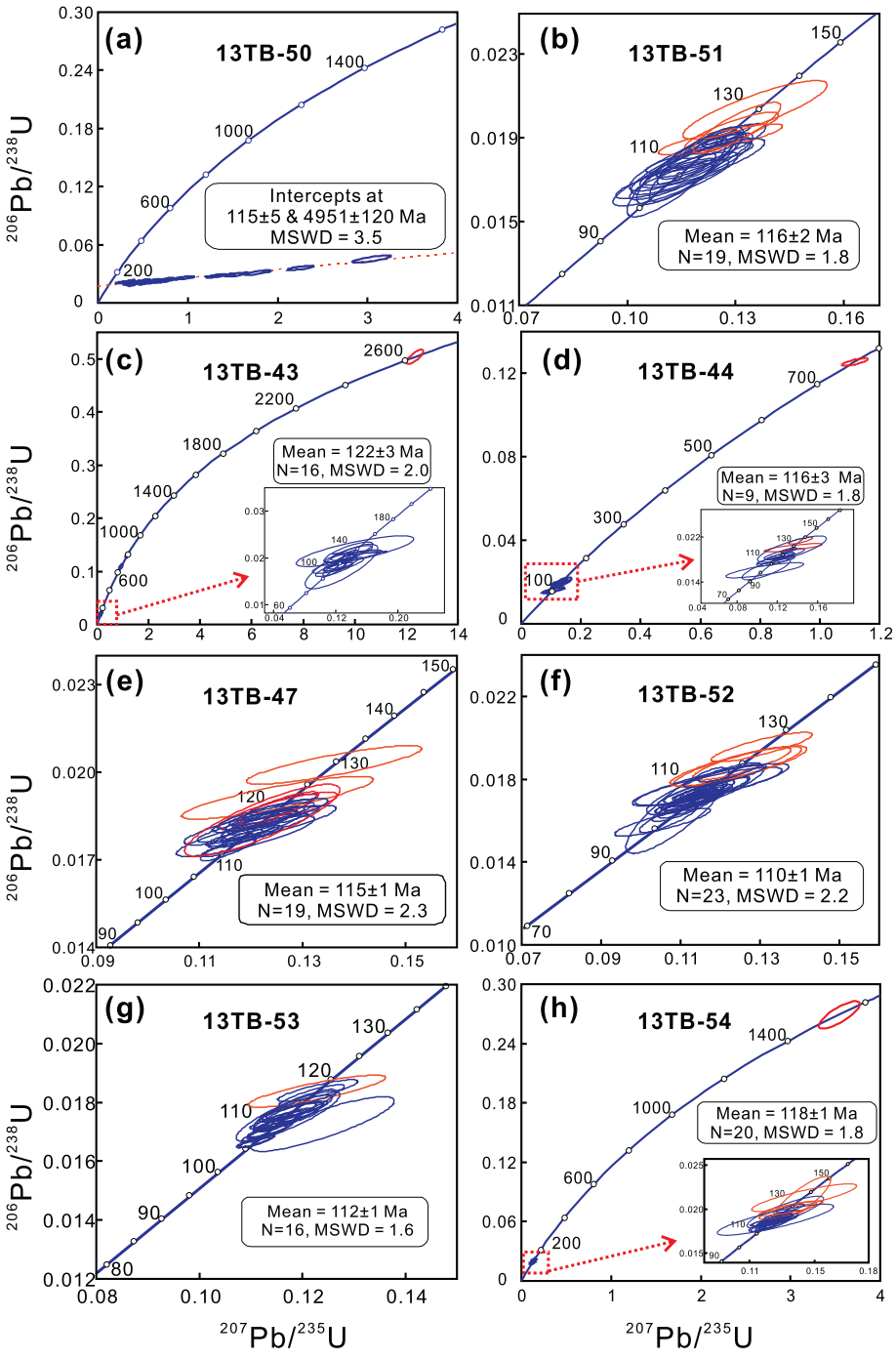

Fig. 7. LA-ICP-MS zircon U—Pb concordia plots for the representative samples from the Lushui-Pianma Batholith. The blue circles represent the data used to calculate concordia age, while the red circles represent the data from inherited or xenocrystal zircons.

4.2. Zircon chemistry and Ti-in-zircon thermometry

Trace element data for all the zircons are reported in Supplementary Table S5. All the zircons from the granitic rocks and the associated mafic enclaves define a single group in terms of their REE contents and normalized REE patterns (Fig. 9). Their prominent enrichment in heavy rare earth elements (HREE) relative to light REE (LREE), combined with their positive Ce and negative Eu anomalies, are typical features of magmatic zircons in igneous rocks (Fig. 9). Such characteristics also suggest that the zircons of the mafic enclaves were most likely crystallized from a same parental magma as the host granitoids, but were affected by the late period of magmatic heat.

The Ti-in-zircon thermometer for the zircons with young crystallization ages was calculated based on the method of Watson et al. (2006). As a whole, the zircons from the enclave have higher Ti-in-zircon temperatures than those from the host and deformed granitic rocks (Supplementary Table S5). It is also noted that the calculated temperatures of all zircons from the enclave along with minor from the granitoids are above 800 °C, and even some higher than 830 °C (Supplementary Table S5).

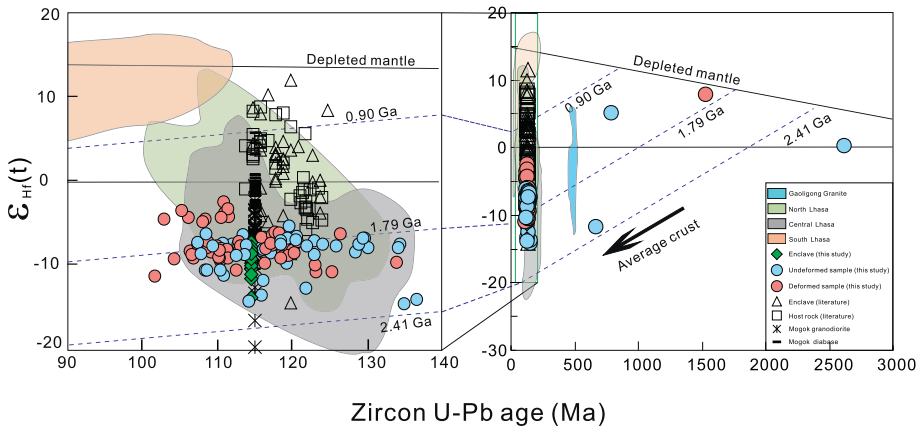

Fig. 8. Relationship between $\varepsilon_{Hf}(t)$ values and U—Pb ages for the zircons from the Lushui-Pianma Batholith. Hf isotopic compositions of chondrite and depleted mantle are from BlichertToft and Albarede (1997) and Vervoort and Blichert-Toft (1999), respectively. The shades representing the data of granitic rocks from Gaoligong granite, North Lhasa, Central Lhasa and South Lhasa are from Zhu et al. (2009). The literatures, and the Mogok granodiorite and Mogok diabase are from Zhu et al. (2017b) and Chen et al. (2016), respectively.

4.3. Major and trace element data

4.3.1. Mafic enclave

The mafic enclaves are characterized by low SiO_2 and high MgO, CaO, $Fe_2O_3^T$, P_2O_5 and TiO_2 contents (Supplementary Table S3). They are gabbroic in composition and have lower K_2O contents than the granitic rocks with an exception of sample 13TB-47 (Fig. 10a), showing a metaluminous nature (Fig. 10b). But compared with the less evolved granites with $SiO_2 < 70$ wt%, the enclaves show slightly lower Cr and Ni contents (Supplementary Table S3). Such signatures are also similar to those of the mafic enclaves having lower Cr and Ni contents than its host granites in the batholiths of the central-southern Tengchong Terrane (Zhu et al., 2017b). An additional striking feature is that the mafic enclaves contain higher Nb contents than all the granitic rocks (Supplementary Table S3). This is consistent with the observation that the former contains a larger amount of amphiboles than the latter. On the SiO_2-variation diagrams (Fig. 11), the mafic enclaves and the host granitoids define a negative correlation between Al_2O_3, MgO, $Fe_2O_3^T$, CaO, P_2O_5, TiO_2 and SiO_2.

In the chondrite-normalized REE plot (Fig. 12a), the mafic enclaves display a similar pattern to those granitic rocks with a pronounced enrichment of light REE relative to heavy REE resulting in La/Yb_n ratios from 4.7 to 13.5, although their LREE fractionation relative to HREE is much weaker than the host granites. Compared with the granitoids, the mafic enclaves show slightly weaker Eu negative anomalies, with $Eu/Eu^* = 0.72–0.77$ (Fig. 12a). Likewise, their primitive mantle-normalized trace element patterns are compatible with those of the host granites, with marked troughs in Ba, Nb, Ta, Sr, P, and Ti (Fig. 12b). A difference between the mafic enclaves and the host is also visible, for instance, the Zr and Hf of the former display more pronounced negative anomalies than those of the latter (Fig. 12b). Compared with the coeval mafic enclaves, the rare and trace element patterns of the LP mafic enclaves are similar to those in the central-southern batholiths of the Tengchong Terrane (Zhu et al., 2017b).

4.3.2. Granite

All the granitic rocks including the undeformed and deformed samples in the LP area have variable major element contents (Supplementary Table S3) and high total alkali ($K_2O + Na_2O$) contents (6.0–8.7 wt %). Their wildly medium K_2O/Na_2O ratios (0.4–2.0) and K_2O contents show that most of them are high-K calc-alkaline series except for one sample with a medium-K calc-alkaline affinity (Fig. 10a). Their A/CNK values (mol. $Al_2O_3/(CaO + K_2O + Na_2O)$) ranging from 0.9 to 1.1, indicate metaluminous to slightly peraluminous nature (Fig. 10b; Clemens, 2003; Sylvester, 1998). The higher Na_2O contents (2.7–4.2 wt%) of the less evolved samples than those of S-type granites (Supplementary Table S3), coupled with the negative correlation between P_2O_5 and SiO_2 (Fig. 11e), suggest an affinity to I-type granite (Chappell and White, 2001). The pervasive presence of amphibole in the less evolved granitoids (Fig. 4a, b, c) also lend strong support to an I-type nature. Akin to the coeval granites in the Menglian and Xiaotang batholiths in the central-southern Tengchong Terrane (Zhu et al., 2017b), the less evolved LP samples also show a common Na-rich feature.

All the granitoids display similar chondrite-normalized REE patterns, showing enrichment in LREE (i.e., $(La/Yb)_{CN} = 5.2–20.2$) and prominent negative Eu anomalies ($Eu/Eu^* = 0.08–0.73$; Fig. 12a). In the primitive mantle-normalized spidergram, they are depleted in Ba, Nb, Ta, Sr, P, and Ti (Fig. 12b). Overall, the geochemical signatures of the LP granitoids resemble those of the granitic batholiths of the central-southern Tengchong Terrane (Zhu et al., 2017a).

4.4. Whole-rock Sr—Nd isotopes

All the representative host (undeformed) and deformed granites have high and variable $^{87}Sr/^{86}Sr$ ratios (0.713338–0.735329) and low $^{143}Nd/^{144}Nd$ ratios (0.512037–0.512140) (Supplementary Table S4). Their initial $^{87}Sr/^{86}Sr$ ratios and ε_{Nd} (t) values vary from 0.708845 to 0.71085 712 and from −10.54 to −8.40, respectively, which are different from those of the Gangdese batholith in the southern Lhasa (Fig. 13). Their T_{DM2} model ages are in the range of 1.49–2.15 Ga (Supplementary Table S4), similar to those in the southern part of the Tengchong Terrane (Zhao et al., 2016).

One representative mafic enclave display similar Sr—Nd isotopic compositions to its host and the deformed granites. Its initial $^{87}Sr/^{86}Sr$ ratio and $\varepsilon_{Nd}(t = 115\ Ma)$ value are of 0.712074 and −9.84, respectively, with a corresponding T_{DM2} model age of 1.70 Ga (Supplementary Table S4; Fig. 13).

5. Discussion

5.1. The spatio-temporal pattern and nature of the Cretaceous magmatism

As stated above, the Cretaceous granitic rocks are cropped widely out in the Tengchong Terrane (e.g., Xie et al., 2016; Zhu et al., 2017a). Based on the summary of the available zircon U—Pb dating results published, Xie et al. (2016) have concluded that the Cretaceous–Eocene magmatism shows a spatial migration from east to west. That is, the Early Cretaceous granitic rocks were emplaced mainly to the east of the GTDF and did not cross the GSZ, while the Late Cretaceous granitic magmatism was concentrated to the west of the GTDF (Fig. 2). In fact,

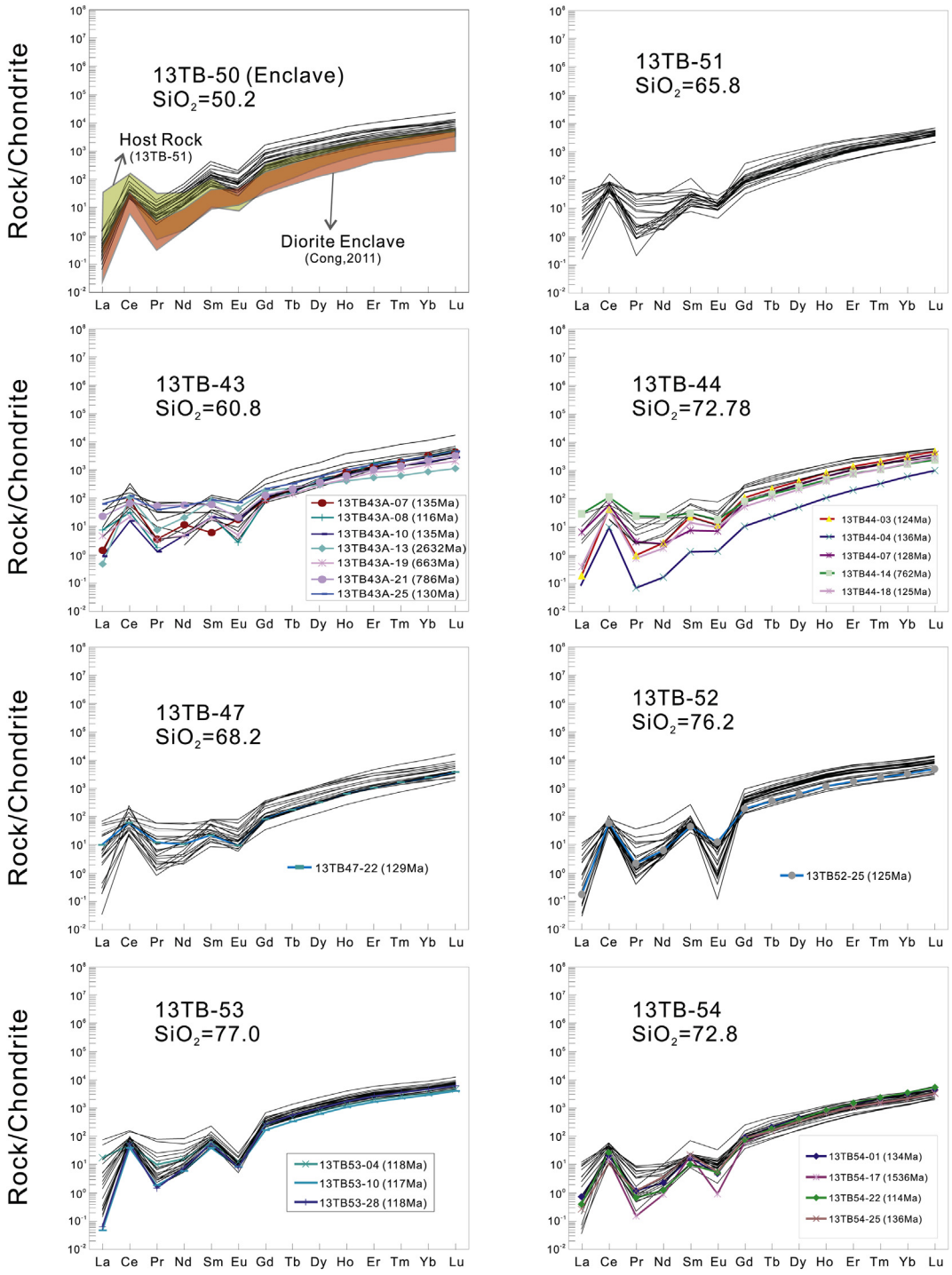

Fig. 9. Chondrite-normalized REE patterns of representative zircon grains from the Lushui-Pianma Batholith.

recent studies have demonstrated that some Early Cretaceous granitoids are also present in the Baoshan Terran to the east of the GSZ (Tao et al., 2010). Moreover, some Late Cretaceous granitic rocks were identified between the GTDF and GSZ, and even minor developed to the east of the GSZ (Xie et al., 2016). More importantly, our zircon U—Pb dating results reveal that minor Early Cretaceous granitic rocks that had been strongly deformed after their emplacement also occur within the GSZ, although increasing numbers of the Early Paleozoic granitic rocks have also been identified mainly in the south of this zone in recent years (Li et al., 2012b; Wang et al., 2013; Zhao et al., 2017a). Accordingly, it is noticeable that the Cretaceous granitic magmatism should have developed in the whole Tengchong Terrane, and part within the GSZ (so-called Lushui-Longlin-Ruili suture zone) and even southwards into the Mogok metamorphic zone of Myanmar (Chen et al., 2016) and eastwards into the Baoshan terranes (Tao et al., 2010). Such a feature does not indicate a clear spatial and temporal zoning pattern as suggested by Xie et al. (2016). By contrast, the Early Cretaceous granitic magmatism could be more widespread than observed at present. The LP batholith should include these strongly deformed granitic rocks within the GSZ such as the studied samples (Fig. 2).

Alternatively, from a consideration of the sole granitic batholith, the LP granitic batholith extends northwards to the boundary between Yunnan and Tibet provinces with an outcrop length of >400 km and largest width of ~50 km in Yunnan Province (YNBGMR, 1990). Spatially, the

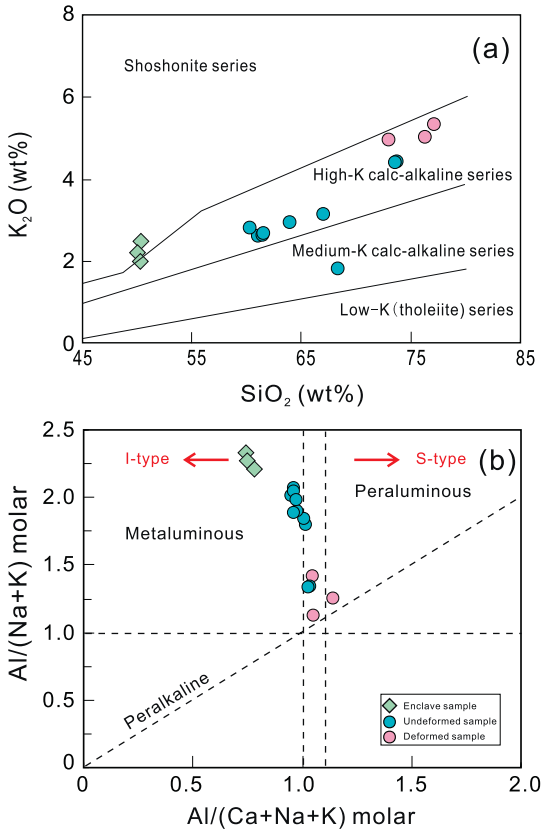

Fig. 10. (a) K_2O versus SiO_2 (after Winchester and Floyd, 1977), and (b) molar Al/(K + Na) versus Al/(Ca + Na + K) diagrams (after Chappell and White, 1992).

granitoids in the east and west sections of the LP batholith have slightly older emplacement ages than those in the center (Fig. 3). Such a pattern is also similar to those in the Menglian and Xiaotang batholiths to the south of it (Fig. 2; Xie et al., 2016; Zhu et al., 2017b). Whether they were the products of continuous or episodic granitic magmatism in the study area in the Early Cretaceous needs further investigation.

Except for the new recognition on the spatio-temporal distribution pattern of the Cretaceous granitic magmatism in the Tengchong Terrane, geochemical signatures of the LP batholith in this study, together with the Menglian and Xiaotang batholiths in the south (Zhu et al., 2017b), mostly show an affinity to I-type granite with a common Na-rich nature (Fang et al., 2018; Zhu et al., 2015). This is distinctly inconsistent with the previous expectation that the Early Cretaceous granitic rocks in the Tengchong Terrane is dominated by similarly peraluminous S-type granites (Xie et al., 2016; Xu et al., 2012) to those of the northern magmatic belt in the Tibetan Plateau (Harris et al., 1990; Kapp et al., 2005). In fact, such Na-rich I-type granites with an Early Cretaceous age also developed in the Mogok metamorphic belt in Myanmar (Chen et al., 2016), as the southern extension of the GSZ.

5.2. Magma origin and petrogenesis

5.2.1. Mafic enclave

Many granitoid intrusions generally host different types of mafic microgranular enclaves (MMEs) as fine-grained, dark-colored and round inclusions, but the origins of the MMEs remain controversial despite they are trapped within a same granitic pluton. Collectively, they can be the residual materials (restites) which successively unmix from the melt during the rise of a crystal mush from its source region (e.g., Chappell and White, 1992), or the products of magma mixing and/or mingling of mantle- and crust-derived magmas (e.g., Jiang et al., 2013; Shaw and Flood, 2009), or the results of crystallization of a coeval magma that give rise to the host granitoids and has a similar source to that of the host granitoids (e.g., Donaire et al., 2005; Flood and Shaw, 2014).

For the restite origin, a vital feature is that the linear chemical variations are observable between the MMEs and their host granites (e.g., Chappell and White, 1992). The composition gap between the MMEs and host granites in the LP batholith is obvious as shown in Fig. 11. Moreover, all the MMEs have lower Cr and Ni contents than their corresponding host granitic rocks in the Tengchong Terrane (this study and published papers; Zhu et al., 2015, 2017b). These characteristics do not accord with a restite origin. Indeed, most of the MMEs as a restite material have been identified to be hosted mainly within the S-type granites (Chappell and White, 2001; Vernon, 2007), and such MMEs generally show a metamorphic or residual sedimentary fabric (Chappell and White, 2001; Vernon, 2007). An igneous origin for the MMEs in the LP region, such as the presence of abundant magmatic hornblendes and biotites (Fig. 4), rules out the restite model.

Magma mixing and/or mingling is a common process in generating mafic to felsic magmas worldwide. This mechanism has thus been popularly invoked to account for the origin of the MMEs within the granitoids, particularly for the MMEs characterized by the igneous textural features, finer grain size and chilled margins, and having different isotopic compositions from their host granitoids (e.g., Shaw and Flood, 2009), although no cogenetic mafic rocks are observed at available exposure level (e.g., Ferla and Meli, 2006). In the case of the LP MMEs in this study, their igneous texture and finer grain size, and monzogabbroic composition with low SiO_2 (49.25–49.52 wt%) and high $K_2O + Na_2O$ (5.27–5.71 wt%) contents seem to resemble the features of magma mixing and/or mingling. However, no observable chilled margin (Fig. 4f) and isotopic differences (Supplementary Tables S2 and S4; Figs. 8 and 14) between the MMEs and their hosts are incompatible with a mixing origin. Furthermore, the magma mixing and/or mingling model is assumed that the MMEs represent the mantle-derived mafic melt (e.g., Vernon, 2007). The MMEs in the LP batholith have lower Cr and Ni contents (Cr < 8 ppm and Ni < 5 ppm) relative to the host granites (Cr = 11.2 ppm and Ni = 5.4 ppm) (Supplementary Table S3; Fig. 11g, f), and lack pyroxenes that commonly occur in the basaltic rocks, indicating that the parental magma of the MMEs could not be derived from the mantle. Although the coeval mantle-derived diabases were identified recently in the Mogok metamorphic belt as the southern extension of the Tengchong Terrane (Chen et al., 2016), the striking chemical and isotopic distinctions between the LP MMEs and the Mogok diabases (Chen et al., 2016) imply that the mantle-derived melts were not involved in the LP MMEs but rather only contributed its heat (also see discussion as follows). In this regards, the magma mixing and/or mingling model is thus impossibly responsible for the LP MMEs. The absence of complex oscillatory zoning and repeated resorption of plagioclase and corroded K-feldspar and quartz xenocrysts in the LP enclaves also argue against the magma mixing model (Bonin, 2004; Vernon, 2007).

By contrast, the geochemical and petrological characteristics of the LP MMEs can indicate a cognate origin from crystallization of a coeval magma that gave rise to the host granitoids (e.g., Donaire et al., 2005; Flood and Shaw, 2014). Considering the fact that the LP MMEs did not represent the mantle-derived melts as discussed above, their significantly similar trace element and Hf isotopic compositions in zircons and whole-rock Nd isotopic compositions to those of their hosts (Supplementary Tables S2 and S4; Figs. 8 and 14), clearly suggest a derivation from a common source region. In addition, the presence of poikilitic microstructure and similar mineral assemblages of the LP MMEs to the host granites (Fig. 4b, c) lend strong support to a cognate origin (e.g., Donaire et al., 2005; Flood and Shaw, 2014). Taken together, based on the absence of the coeval mantle-derived rocks (such as basalts, gabbros, etc.) in or nearby the granitoid batholith, the most feasible explanation for the broad similarity in the mineral assemblages and

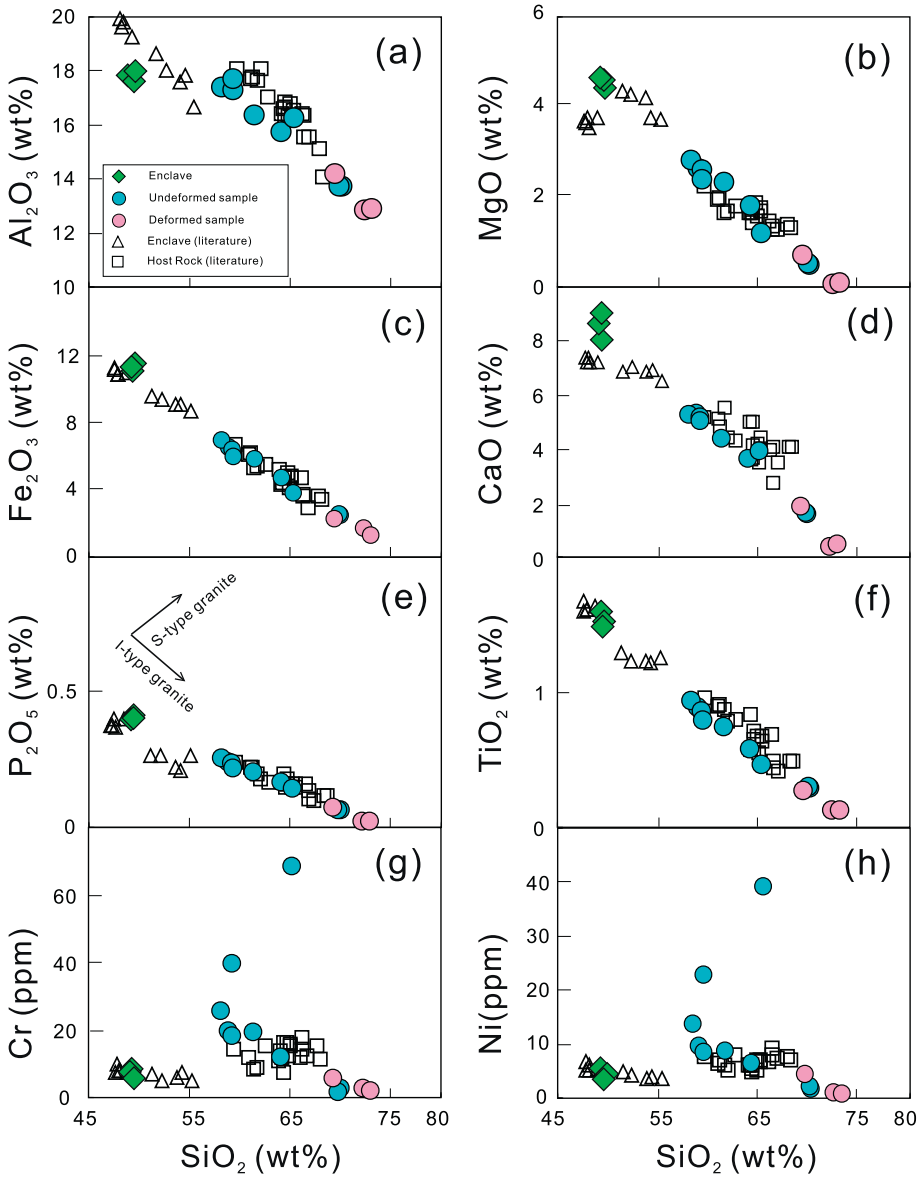

Fig. 11. Harker variation diagrams for the Lushui-Pianma granitoids and its enclave.

Hf—Nd isotopes between the MMEs and the host granites in the LP batholith is that the LP mafic enclaves were crystallized from the coeval, cognate magmas via crystal accumulation (Flood and Shaw, 2014) or chilled margin processes (Donaire et al., 2005), or a crystallization process by rapid cooling within the host granitoid magma operating at the margins of magma conduits (e.g., Donaire et al., 2005).

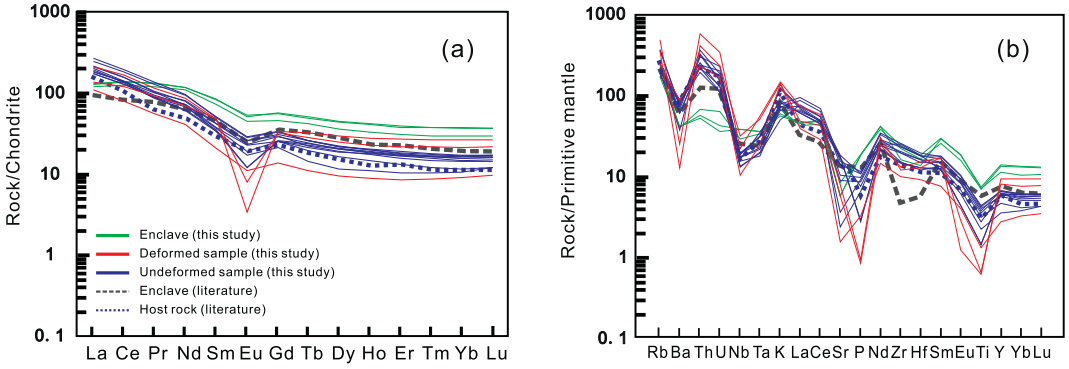

Fig. 12. (a) Chondrite-normalized REE patterns and (b) Primitive mantle-normalized spider diagrams for the samples from the Lushui-Pianma Batholith and its enclave. Normalizing values of chondrite and primitive mantle are from Sun and Mcdonough (1989) and Taylor and Mclennan (1985), respectively. The literaure data are from Fang et al. (2018) and Zhu et al. (2015, 2017b).

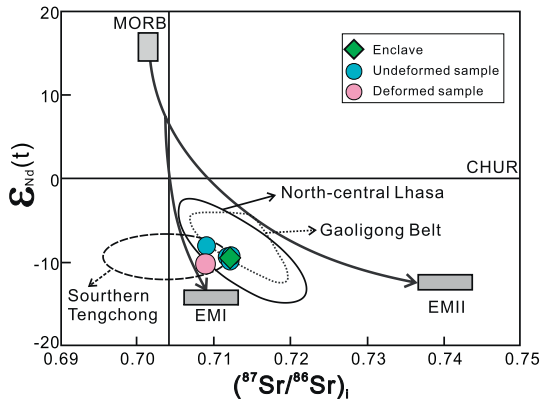

Fig. 13. $\varepsilon_{Nd}(t)$ versus initial $^{87}Sr/^{86}Sr(t)$ ($t = 115$ Ma). The data of the Gaoligong Shear Belt, northern-central Lhasa and southern Tengchong are from Zhao et al. (2016), Zhu et al. (2009) and Zhu et al. (2015).

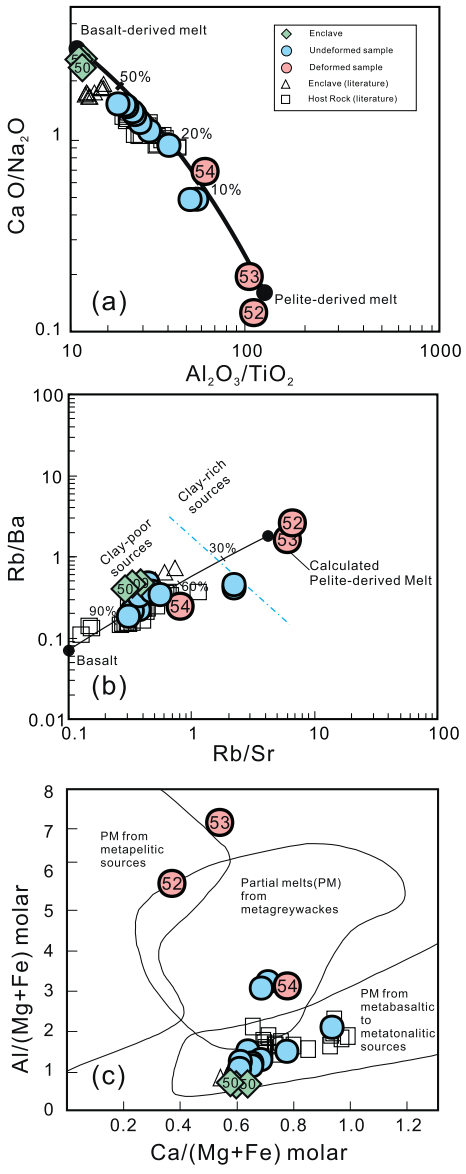

Fig. 14. (a) CaO/Na_2O versus Al_2O_3/TiO_2 and (b) Rb/Ba versus Rb/Sr diagrams. The calculated shale- and greywacke-derived melts are from Sylvester (1998). (c) Molar Al/(Mg + Fe) versus Ca/(Mg + Fe) diagram. The empty squares represent the literature data from Zhu et al. (2017b).

Previous studies have demonstrated that the pervasive fine-grained and poikilitic texture of enclaves (Fig. 4c), and the rounded interfaces and diffuse contacts with its host (Fig. 4f) reflect the quenching of magma when brought into close proximity to the cooler magma in the dynamic magma chamber (e.g., Farner et al., 2014). Additionally, the high modal ferromagnesian mineral contents including hornblende and biotite (>50 vol%) in the LP MMEs have also been regarded as the products of cognate origin (Donaire et al., 2005) since the mafic phases nucleate more quickly than quartz and feldspar (Weinberg et al., 2001). To sum up, all the above-mentioned attributes of the LP MMEs agree with a cognate origin that they were crystallized from a coeval intermediate-felsic magma chamber.

In a consequence, the cognate origin can also be a pervasive mechanism responsible for some MMEs entrained in the calc-alkaline granitoid rather than usually used as evidence for magma mixing and/or mingling between mantle-derived mafic and crustal-derived felsic magmas (Schonenberger et al., 2006).

5.2.2. Granite

As stated above, most of the LP granitoids are metaluminous (A/CNK < 1.1) and Na-rich barring the highly evolved granite (including undeformed sample and strongly deformed samples having A/CNK > 1.1 and $Na_2O/K_2O > 1.0$). Na-rich granitic magma can be produced through H_2O-fluxed melting of metapelite under condition of high pressure (~10 kbar; Douce and Harris, 1998), or partial melting of metabasic rock such as amphibolite (Richards and Kerrich, 2007).

All the less evolved dioritic rocks characterized by metaluminous nature, low Rb/Sr and Rb/Ba ratios and Al_2O_3 contents, and high MgO and FeO_t contents, are markedly distinguishable from the metapelite-derived melt as shown in Fig. 14. Such signatures, coupled with an affinity to I-type granite, indicate an origin from a partial fusion of metaigneous rocks. As the cognate products of the LP granitoids as discussed above, the MMEs most likely reflect their source nature. Their high CaO and TiO_2 contents and low Al_2O_3 contents coincide with the basalt-derived melt (Fig. 14), indicating their parental magma was derived from partial melting of basaltic protoliths.

Na-rich granitoids are most widespread in the Archean, such as TTGs (Tonalite-Trondhjemite-Granodiorite; e.g., Martin et al., 2005), and some also develop in the Phanerozoic, particularly the adakitic rocks (Wang et al., 2005). Although the origin of the two types of Na-rich granitic rocks remains controversial, including partial melting of thickened mafic lower crust (garnet-bearing amphibolite or eclogite) or subducting oceanic slab, their source rocks are composed mainly of basic rocks (e.g., Martin et al., 2005). Moreover, they are commonly characterized by high Sr contents (>400 ppm) and Sr/Y ratios (>20) and low Y (<19 ppm) and Yb (<1.8 ppm) contents (Martin et al., 2005) with no Eu anomaly. In this respect, the low Sr contents (<400 ppm) and Sr/Y ratios (<20) and high Y (>19 ppm) and Yb (>1.8 ppm) contents of the LP Na-rich granitoids in this study with conspicuous negative Eu anomalies ($Eu^{\#} < 0.8$; Supplementary Table S3) are clearly inconsistent with the Archean TTGs and Phanerozoic adakitic rocks. This hints that the LP Na-rich granitoids were not derived from partial melting of the thickened lower crust or the subducting oceanic slab, but rather the results of partial melting of middle-lower crustal metabasalts at depth of <40 km.

Alternatively, the wide range of zircon Hf isotopic compositions of the LP Na-rich granitoids suggests that their source rocks are heterogeneous. Minor inherited zircons with different ages were identified in these granitic rocks (Supplementary Table S1) also argue for such a proposition. In combination with their two-stage Hf model ages (Supplementary Table S2), it is most likely that their source are dominated by the Mesoproterozoic metabasic rocks with minor Archean rocks as revealed by the Archean inherited zircon from the LP granitoids, which is different from those in the batholiths in the central-southern Tengchong Terrane with a relatively younger source rocks (Zhu et al., 2017b). This source materials of the LP granitoids likely correspond to

the basement rocks of the Gaoligon Group in the Tengchong Terrane (YNBGMR, 1990).

In addition, the geochemical variations of the LP granitoid rocks reflect the results of crystal fractionation during magmatic evolution, which is a general process of granitic magmatism (Clemens, 2003). For instance, the increasing Ba and varying Rb contents with increasing Sr contents, along with deceasing Ba/Sr ratios with increasing Ba contents (not shown) and the notable negative Eu anomaly and depletion in Ba, Sr, Eu, P, Nb, and Ti, imply the fractional crystallization of K-feldspar, biotite, apatite, Ti-rich minerals and ilmenite during the process of magma evolution (Clemens, 2003; Sylvester, 1998; Wang et al., 2013 and references therein).

5.3. Tectonic regime

As discussed above, the spatio-temporal distribution pattern, rock associations, and geochemical and isotopic signatures of the Cretaceous granitic rocks in the Tengchong Terrane are closely comparable with those in the northern Lhasa Terrane, likely implying that they were generated in a same tectono-magmatic regime during the Cretaceous times. More importantly, the similarities including the magmatic activity, the paleontology and stratigraphy features to those in the central-northern Lhasa Terrane since the Early Paleozoic (e.g., Xie et al., 2016 and references therein), led most researchers to believe that the Tengchong Terrane is a southern extension of the Lhasa Terrane (Xu et al., 2012; Zhao et al., 2016; Zhao et al., 2017c), and that both terranes have experienced same or comparable tectonic evolutionary history since that times (Song et al., 2007; Xie et al., 2016).

Consequently, most workers invoke the similar genetic models responsible for the early Cretaceous magmatism in the Lhasa Terrane to account for the generation of the early Cretaceous granitic magmatism in the Tengchong Terrane, although some geodynamic differences between them based on distinct observations. Taken together, they include (1) low-angle northward subduction of the Neo-Tethys oceanic lithosphere (Coulon et al., 1986), (2) southward subduction of the Bangonghu–Nujiang oceanic slab (Zhu et al., 2009; Zhu et al., 2011; Zhu et al., 2015; Zhu et al., 2017a), (3) melting of over thickened crust due to the Lhasa-Qiangtang continental collision (Xu et al., 2012), or crustal anatexis related to mantle attenuation and associated asthenospheric upwelling following Lhasa-Qiangtang continental collision (Harris et al., 1990), and (4) northward underthrusting of the Lhasa terrane beneath the Qiangtang terrane along the Bangong suture during low-angle subduction of Neo-Tethys oceanic lithosphere (Kapp et al., 2005).

Despite some differences between them, these models were mainly based on a common hypothesis that the LLRF between the Tengchong and Baoshan terranes represents the southward continuation of the Bangong–Nujiang Ocean (BNO) within the Tibetan Plateau (Xie et al., 2016; Xu et al., 2012; Zhu et al., 2015; Zhu et al., 2017a). The proposed crucial line of evidence is that the ultramafic massifs exposed along this fault were traditionally regarded as the important component of the Meso-Tethys Ocean, or the BNO (e.g., Liu et al., 2002; YNBGMR, 1990). In fact, the subsequent study, especially for the Sr-Nd-Pb-Os isotopic compositions of these ultramafic peridotites, demonstrated that they were not the fragments of oceanic lithosphere but rather the components of the old sub-continental lithospheric mantle (Chu et al., 2009). Moreover, no other crucial components of typical oceanic ophiolitic remnants have been recognized so far, implying that the LLRF between the Tengchong and Baoshan terranes did not represent the suture zone of an ancient ocean. This also precludes the possibility that the fault was the southern continuation of the BNO of the Tibetan Plateau. By contrast, most recently, the identification of the typical oceanic ophiolitic units in the Myitkyina of Eastern Myanmar, including the oceanic plagiogranites with the formation ages of ~180–165 Ma (Liu et al., 2016a; Yang et al., 2012), and mantle peridotites of oceanic lithosphere (Liu et al., 2016b), along with the new recognization of the oceanic cherts and pillow basalts (Liu et al., 2016a), obviously indicate the existence of an ancient ocean. More importantly, these ophiolitic fragments are geochronologically, petrologically and geochemically same as those cropped out along the Bangong-Nujiang suture zone within the Tibetan Plateau (e.g., Shi, 2007; Wang et al., 2016 and references therein), implying a similar type of ocean basin in the Myitkyina of Eastern Myanmar to the BNO within the Tibetan Plateau. It is thus most likely that the BNO in the Tibetan Plateau extended southward into the Myitkyina-Mogok area in Myanmar (Liu et al., 2016a), which is located to the west of the Tengchong Terrane (Fig. 1b). In this case, the rock-forming geodynamic regime of the Early Cretaceous granitic rocks in the Tengchong Terrane should be reevaluated.

Based on the above discussion, it is quite obvious that these Early Cretaceous granitic rocks in the Tengchong Terrane should be attributed to be the products of the evolution of the Myitkyina Tethys Ocean of Myanmar. Due to the absence of the associated geological data except for the study of the ophiolite-related rocks in the Eastern Myanmar (Liu et al., 2016a; Liu et al., 2016b; Yang et al., 2012), determining whether these granitoids were generated in a subduction-related island arc environment or post-collision regime appears to be difficult. The following observations, however, can provide an important constraint on the geodynamic setting for the Early Cretaceous magmatism in the Tengchong Terrane. (1) The Jurassic and Cretaceous strata are commonly absent in the whole Tengchong Terrane (YNBGMR, 1990), likely indicating that a regional uplift and erosion had took place at least in the Cretaceous era. (2) The Cretaceous strata dominated by the purplish-red sandstones with the conglomerates in the lowermost part (Luxi Geological Map at 1:200,000 scale; YNBGMR, 1990) is present only in the Santaishan of Luxi area to the east of the LLRF (Fig. 1b), in which some ultramafic peridotites previously regarded as the Jurassic ophiolites are cropped out (Mo et al., 1998; YNBGMR, 1990). More importantly, the Cretaceous sandstones overly unconformably the late Jurassic purplish red sandstone (the Nongkan Formation-J_3n; YNBGMR, 1990), implying that the sedimentation developed in the continental facies environment and the uplift should have taken place during the late Jurassic-Early Cretaceous. (3) Some depleted mantle-derived magmas with the emplacement ages of ~120–110 Ma and the zircon $\varepsilon_{Hf}(t)$ values of >5.0 have been recognized recently in the Tengchong Terrane, such as some mafic enclaves hosted within the Early Cretaceous granitoids in the Tengchong-Lianghe region (Zhu et al., 2017b) and the diabases in the Mogok metamorphic belt of Myanmar (Chen et al., 2016), reflecting the onset of the extension-related mantle-derived magmatism in the Early Cretaceous. (4) The high Ti-in-zircon saturation temperatures of the mafic enclaves hosted within the LP granitoids (up to 900 °C this study) and Laoxiangkeng pluton (up to 1000 °C; Fang et al., 2018) also lend strong support to a mantle contribution to the generation of the Early Cretaceous granitic rocks in the Tengchong Terrane. Collectively, all the above features point to the fact that the Meso-Tethys Ocean basin had been closed at least in the Early Cretaceous and a post-collisional extensional regime related to the upwelling and subsequent partial melting of the depleted asthenospheric mantle had occurred. Hence, the most feasible mechanism responsible for such scenario can be ascribed to the post-collisional lithospheric extension.

5.4. Geodynamic mechanism

From a consideration of the linear distribution of most Early Cretaceous magmatism in the Tengchong Terrane along the LLRF, except for minor developed in the Myitkyina-Mogok ophiolitic belt (our unpublished data), a post-collisional slab breakoff model is the most persuasive mechanism to account for such magmatic pattern. Slab breakoff generally results in a narrow linear zone of magmatism, the uplift that propagates along strike, and moderate amounts of erosional products

in intramontane basins (Von Blanckenburg and Davies, 1995). Moreover, the mechanism has the potential to cause upwelling of the asthenosphere that would perturb the original thermal gradient and lead to lithospheric extension and large volumes of magma generation (Bonin, 2004).

In this scenario, following slab breakoff, a detached part of the lithosphere would sink into the mantle and force some mantle materials down with it. Hot asthenosphere would rise and heat the mantle directly above the descending slab as it sinks deeper. Heat from the asthenospheric mantle would be transferred to the mantle lithosphere by conduction, and this would trigger partial melting of the overlying enriched wedge mantle (Von Blanckenburg and Davies, 1995). The basaltic magmas formed by this melting would rise into the crust, where they further induce large-scale crustal melting, resulting in granitic magmatism (Atherton and Ghani, 2002; Von Blanckenburg and Davies, 1995). Owing to the thickened nature of the crust, magmatism, particularly in the early stage of the slab breakoff (ca. 130 Ma), would be dominated by felsic rocks. With the successive crustal fusion and lithospheric thinning, a large scale of partial melting of the lithospheric mantle also commenced to take place. Underplating of basic magma beneath the middle-lower crust would further trigger more intensively crustal fusion and granitic magmatic flare-up during ~120–110 Ma. Meanwhile, part of basic magmas intruded into the early emplaced granitic plutons, such as the ~120 Ma Yinmabin diabase dyke swarm in the Mogok metamorphic belt of Myanmar (Chen et al., 2016).

6. Conclusions

Geochronological and geochemical data for the Early Cretaceous Lushui-Pianma granitoids and its mafic enclaves in the Tengchong Terrane, coupled with previously published results, allow us to reach the following conclusions:

1) The Lushui-Pianma granitoids, including the undeformed batholith and the deformed rocks from the Gaoligong shear zone, were emplaced in the Early Cretaceous ranging from ca. 122 Ma to 110 Ma. The mafic enclave hosted in the undeformed granite record a same timing of thermal event (~115 Ma) as the emplacement timing of its host granite.
2) The Early Cretaceous granitic rocks in the Tengchong Terrane are dominated by I-type granites, different from the predominant S-type granites in the Northern magmatic belt in the Lhasa Terrane. The Lushui-Pianma granitoids were derived from partial melting of the Mesoproterozoic basement rocks dominated by the metabasalts, while the mafic enclaves were cognate with its host granitoids.
3) The Early Cretaceous granitic rocks in the Tengchong Terrane were the products of the evolution of the Myitkyina Meso-Tethys Ocean in the eastern Myanmar rather than the Bangong-Nujiang Ocean between the Tengchong and Baoshan terranes. And their generation was related to post-collisional slab breakoff.

Supplementary data to this article can be found online at https://doi.org/10.1016/j.lithos.2018.08.017.

Acknowledgments

We would like to acknowledge Y.S. Mao for helping for the field trip, and X.Y. Fang, B.B. Liu for help with the analysis of the zircons, and Prof. Liang Qi for his help for trace element analysis. We also thank two anonymous reviewers and editor Xianhua Li for their constructive comments. This research has received financial support from the Natural Science Foundation of China (Grant Nos. 41490613, and 41672058). This is a contribution from the Guangzhou Institute of Geochemistry, Chinese Academy of Sciences (GIG, CAS; No. xxx) and CAS Hundred Talents Project to Jian-Feng Gao (Y5CJ038000).

References

Andersen, T., 2002. Correction of common lead in U–Pb analyses that do not report 204 Pb. Chem. Geol. 192, 59–79.
Atherton, M.P., Ghani, A.A., 2002. Slab breakoff: a model for Caledonian, Late Granite syncollisional magmatism in the orthotectonic (metamorphic) zone of Scotland and Donegal, Ireland. Lithos 62, 65–85.
Barbarin, B., 1999. A review of the relationships between granitoid types, their origins and their geodynamic environments. Lithos 46, 605–626.
BlichertToft, J., Albarede, F., 1997. The Lu-Hf isotope geochemistry of chondrites and the evolution of the mantle-crust system. Earth Planet. Sci. Lett. 148, 243–258.
Bonin, B., 2004. Do coeval mafic and felsic magmas in post-collisional to within-plate regimes necessarily imply two contrasting, mantle and crustal, sources? A review. Lithos 78, 1–24.
Chappell, B.W., White, A.J.R., 1992. I-type and S-type granites in the Lachlan Fold Belt. Trans. R. Soc. Edinburgh-Earth Sci. 83, 1–26.
Chappell, B.W., White, A.J.R., 2001. Two contrasting granite types: 25 years later. Aust. J. Earth Sci. 48, 489–499.
Chen, X.J., Xu, Z.Q., Sein, K., Meng, Y.K., Cai, Z.H., 2016. The Early Cretaceous tectonic magmatism in the Mogok District, central Myanmar, and its implication for the evolution of Tethys. Acta Geol. Sin. 3060–3080 (in Chinese with English abstract).
Chu, Z.Y., Wang, W., Chen, F.K., Wang, X.L., Li, X.H., Ji, J.Q., 2009. Os-Nd-Pb-Sr isotopic compositions of the Santaishan ultramafic rock in western Yunnan and its geological significances. Acta Petrol. Sin. 25, 3221–3228 (in Chinese with English abstract).
Clemens, J.D., 2003. S-type granitic magmas – petrogenetic issues, models and evidence. Earth Sci. Rev. 61, 1–18.
Coulon, C., Maluski, H., Bollinger, C., Wang, S., 1986. Mesozoic and Cenozoic volcanic-rocks from central and southern Tibet – ^{39}Ar-^{40}Ar dating, petrological characteristics and geodynamical significance. Earth Planet. Sci. Lett. 79, 281–302.
Donaire, T., Pascual, E., Pin, C., Duthou, J.L., 2005. Microgranular enclaves as evidence of rapid cooling in granitoid rocks: the case of the Los Pedroches granodiorite, Iberian Massif, Spain. Contrib. Mineral. Petrol. 149, 247–265.
Douce, A.E.P., Harris, N., 1998. Experimental constraints on Himalayan anatexis. J. Petrol. 39, 689–710.
Eby, G.N., 1992. Chemical subdivision of the A-type granitoids – petrogenetic and tectonic implications. Geology 20, 641–644.
Fang, Y., Zhang, Y.H., Zhang, S.T., Cao, H.W., Zou, H., Dong, J.H., 2018. Early Cretaceous I-type granites in the Tengchong terrane: new constraints on the late Mesozoic tectonic evolution of southwestern China. Geosci. Front. 9, 459–470.
Farner, M.J., Lee, C.T.A., Putirka, K.D., 2014. Mafic-felsic magma mixing limited by reactive processes: a case study of biotite-rich rinds on mafic enclaves. Earth Planet. Sci. Lett. 393, 49–59.
Ferla, P., Meli, C., 2006. Evidence of magma mixing in the 'Daly gap' of alkaline suites: a case study from the enclaves of Pantelleria (Italy). J. Petrol. 47, 1467–1507.
Flood, R.H., Shaw, S.E., 2014. Microgranitoid enclaves in the felsic Looanga monzogranite, New England Batholith, Australia: pressure quench cumulates. Lithos 198, 92–102.
Griffin, W.L., Wang, X., Jackson, S.E., Pearson, N.J., O'Reilly, S.Y., Xu, X.S., Zhou, X.M., 2002. Zircon chemistry and magma mixing, SE China: in-situ analysis of Hf isotopes, Tonglu and Pingtan igneous complexes. Lithos 61, 237–269.
Griffin, W.L., Belousova, E.A., Shee, S.R., Pearson, N.J., O'Reilly, S.Y., 2004. Archean crustal evolution in the northern Yilgam Craton: U-Pb and Hf-isotope evidence from detrital zircons. Precambrian Res. 131, 231–282.
Harris, N.B.W., Inger, S., Xu, R.H., 1990. Cretaceous plutonism in central Tibet – an example of postcollision magmatism. J. Volcanol. Geotherm. Res. 44, 21–32.
Jiang, Y.H., Jia, R.Y., Liu, Z., Liao, S.Y., Zhao, P., Zhou, Q., 2013. Origin of Middle Triassic high-K calc-alkaline granitoids and their potassic microgranular enclaves from the western Kunlun orogen, northwest China: A record of the closure of Paleo-Tethys. Lithos 156, 13–30.
Kapp, P., Yin, A., Harrison, T.M., Ding, L., 2005. Cretaceous-Tertiary shortening, basin development, and volcanism in central Tibet. Geol. Soc. Am. Bull. 117, 865–878.
Le Maitre, R.W., 2002. Igneous rocks – a classification and glossary of terms. Recommendations of the IUGS Subcommission on the Systematics of Igneous Rocks, 2nd ed. Cambridge University Press, Cambridge.
Li, X.H., Long, W.G., Li, Q.L., Liu, Y., Zheng, Y.F., Yang, Y.H., Chamberlain, K.R., Wan, D.F., Guo, C.H., Wang, X.C., Tao, H., 2010. Penglai zircon megacrysts: a potential new working reference material for microbeam determination of Hf-O isotopes and U-Pb age. Geostand. Geoanal. Res. 34, 117–134.
Li, Z.H., Lin, S.L., Cong, F., Xie, T., Zou, G.F., 2012b. U-Pb ages of zircon from metamorphic rocks of the Gaoligongshan Group in western Yunnan and its tectonic significance. Acta Petrol. Sin. 28, 1529–1541 (in Chinese with English abstract).
Li, D.P., Luo, Z.H., Chen, Y.L., Liu, J.Q., Jin, Y., 2014a. Deciphering the origin of the Tengchong block, west Yunnan: evidence from detrital zircon U-Pb ages and Hf isotopes of Carboniferous strata. Tectonophysics 614, 66–77.
Li, S.M., Zhu, D.C., Wang, Q., Zhao, Z.D., Sui, Q.L., Liu, S.A., Liu, D., Mo, X.X., 2014b. Northward subduction of Bangong–Nujiang Tethys: insight from Late Jurassic intrusive rocks from Bangong Tso in western Tibet. Lithos 205, 284–297.
Liang, Q., Jing, H., Gregoire, D.C., 2000. Determination of trace elements in granites by inductively coupled plasma mass spectrometry. Talanta 51, 507–513.
Liang, X.R., Wei, G.J., Li, X.H., Liu, Y., 2003. Precise measurement of ^{143}Nd/^{144}Nd and Sm/Nd ratios using multiple collectors inductively coupled plasma mass spectrometer (MC-ICPMS). Geochimica 91–96 (in Chinese with English abstract).

Liu, B.P., Feng, Q.L., Chonglakmani, C., Helmcke, D., 2002. Frame work of Paleotethyan archipelago ocean of western Yunnan and its elongation towards north and south. Earth Sci. Front. 161–171.
Liu, Y.S., Gao, S., Hu, Z.C., Gao, C.G., Zong, K.Q., Wang, D.B., 2010a. Continental and oceanic crust recycling-induced melt-peridotite interactions in the Trans-North China Orogen: U-Pb dating, Hf isotopes and trace elements in zircons from mantle xenoliths. J. Petrol. 51, 537–571.
Liu, Y.S., Hu, Z.C., Zong, K.Q., Gao, C.G., Gao, S., Xu, J.A., Chen, H.H., 2010b. Reappraisement and refinement of zircon U-Pb isotope and trace element analyses by LA-ICP-MS. Chin. Sci. Bull. 55, 1535–1546.
Liu, C.Z., Chung, S.L., Wu, F.Y., Zhang, C., Xu, Y., Wang, J.G., Chen, Y., Guo, S., 2016a. Tethyan suturing in Southeast Asia: zircon U-Pb and Hf-O isotopic constraints from Myanmar ophiolites. Geology 44, 311–318.
Liu, C.Z., Zhang, C., Xu, Y., Wang, J.G., Chen, Y., Guo, S., Wu, F.Y., Sein, K., 2016b. Petrology and geochemistry of mantle peridotites from the Kalaymyo and Myitkyina ophiolites (Myanmar): implications for tectonic settings. Lithos 264, 495–508.
Ludwig, K.R., 2003. ISOPLOT 3.0: A Geochronological Toolkit for Microsoft Excel. Berkeley Geochronology Center Special Publication.
Ma, N., Deng, J., Wang, Q.F., Wang, C.M., Zhang, J., Li, G.J., 2013. Geochronology of the Dasongpo tin deposit, Yunnan Province: Evidence from zircon LA-ICP-MS U-Pb ages and cassiterite LA-MC-ICP-MS U-Pb age. Acta Petrol. Sin. 29, 1223–1235 (in Chinese with English abstract).
Martin, H., Smithies, R.H., Rapp, R., Moyen, J.F., Champion, D., 2005. An overview of adakite, tonalite-trondhjemite-granodiorite (TTG), and sanukitoid: relationships and some implications for crustal evolution. Lithos 79, 1–24.
Metcalfe, I., 2013. Gondwana dispersion and Asian accretion: tectonic and palaeogeographic evolution of eastern Tethys. J. Asian Earth Sci. 66, 1–33.
Mo, X.X., Shen, S.Y., Zhu, Q.W., 1998. Volcanics-Ophiolite and Mineralization of Middle and Southern Part in Sanjiang, Southern China. Geological Publishing House, Beijing.
Richards, J.R., Kerrich, R., 2007. Special paper: Adakite-like rocks: their diverse origins and questionable role in metallogenesis. Econ. Geol. 102, 537–576.
Schonenberger, J., Marks, M., Wagner, T., Markl, G., 2006. Fluid-rock interaction in autoliths of agpaitic nepheline syenites in the Ilimaussaq intrusion, South Greenland. Lithos 91, 331–351.
Shaw, S.E., Flood, R.H., 2009. Zircon Hf isotopic evidence for mixing of crustal and silicic mantle-derived magmas in a zoned granite pluton, eastern Australia. J. Petrol. 50, 147–168.
Shi, R.D., 2007. SHRIMP dating of the Bangong Lake SSZ-type ophiolite: constraints on the closure time of ocean in the Bangong Lake-Nujiang River, northwestern Tibet. Chin. Sci. Bull. 52, 936–941.
Soderlund, U., Patchett, J.P., Vervoort, J.D., Isachsen, C.E., 2004. The Lu-176 decay constant determined by Lu-Hf and U-Pb isotope systematics of Precambrian mafic intrusions. Earth Planet. Sci. Lett. 219, 311–324.
Song, S.G., Ji, J.Q., Wei, C.J., Su, L., Zheng, Y.D., Song, B., Zhang, L.F., 2007. Early Paleozoic granite in Nujiang River of northwest Yunnan in southwestern China and its tectonic implications. Chin. Sci. Bull. 52, 2402–2406.
Steiger, R.H., Jäger, E., 1977. Subcommission on geochronology: convention on the use of decay constants in geo- and cosmochronology. Earth Planet. Sci. Lett. 36, 359–362.
Sui, Q.L., Wang, Q., Zhu, D.C., Zhao, Z.D., Chen, Y., Santosh, M., Hu, Z.C., Yuan, H.L., Mo, X.X., 2013. Compositional diversity of ca. 110 Ma magmatism in the northern Lhasa Terrane, Tibet: implications for the magmatic origin and crustal growth in a continent-continent collision zone. Lithos 168, 144–159.
Sun, S.S., McDonough, W.F., 1989. Chemical and isotopic systematics of oceanic basalts: implications for mantle composition and processes. Geol. Soc. Lond., Spec. Publ. 42, 313–345.
Sun, J., Liu, Z., Zhang, S., Li, X.G., Qi, J.F., 2017. Large-scale removal of lithosphere underneath the North China Craton in the Early Cretaceous: geochemical constraints from volcanic lavas in the Bohai Bay Basin. Lithos 292, 69–80.
Sylvester, P.J., 1998. Post-collisional strongly peraluminous granites. Lithos 45, 29–44.
Tao, Y., Hu, R.Z., Zhu, F.L., Ma, Y.S., Ye, L., Cheng, Z.T., 2010. Ore-forming age and the geodynamic background of the Hetaoping lead-zinc deposit in Baoshan, Yunnan. Acta Petrol. Sinica 26, 1760–1772 (in Chinese with English abstract).
Taylor, S.R., Mclennan, S.M., 1985. The Continental Crust: Its Composition and Evolution, an Examination of the Geochemical Record Preserved in Sedimentary Rocks. Blackwell Scientific Pub.
Vernon, R.H., 2007. Problems in identifying restite in S-type granites of southeastern Australia, with speculations on sources of magma and enclaves. Can. Mineral. 45, 147–178.
Vervoort, J.D., Blichert-Toft, J., 1999. Evolution of the depleted mantle: Hf isotope evidence from juvenile rocks through time. Geochim. Cosmochim. Acta 63, 533–556.
Von Blanckenburg, F., Davies, J.H., 1995. Slab breakoff – a model for syncollisional magmatism and tectonics in the Alps. Tectonics 14, 120–131.
Wang, Q., McDermott, F., Xu, J.F., Bellon, H., Zhu, Y.T., 2005. Cenozoic K-rich adakitic volcanic rocks in the Hohxil area, northern Tibet: lower-crustal melting in an intracontinental setting. Geology 33, 465–468.
Wang, Y.J., Xing, X.W., Cawood, P.A., Lai, S.C., Xia, X.P., Fan, W.M., Liu, H.C., Zhang, F.F., 2013. Petrogenesis of early Paleozoic peraluminous granite in the Sibumasu Block of SW Yunnan and diachronous accretionary orogenesis along the northern margin of Gondwana. Lithos 182, 67–85.
Wang, B.D., Wang, L.Q., Chung, S.L., Chen, J.L., Yin, F.G., Liu, H., Li, X.B., Chen, L.K., 2016. Evolution of the Bangong-Nujiang Tethyan ocean: insights from the geochronology and geochemistry of mafic rocks within ophiolites. Lithos 245, 18–33.
Watson, E.B., Wark, D.A., Thomas, J.B., 2006. Crystallization thermometers for zircon and rutile. Contrib. Mineral. Petrol. 151, 413–433.
Weinberg, R.F., Sial, A.N., Pessoa, R.R., 2001. Magma flow within the Tavares pluton, northeastern Brazil: compositional and thermal convection. Geol. Soc. Am. Bull. 113, 508–520.
Winchester, J.A., Floyd, P.A., 1977. Geochemical discrimination of different magma series and their differentiation products using immobile elements. Chem. Geol. 20, 325–343.
Wu, F.Y., Yang, Y.H., Xie, L.W., Yang, J.H., Xu, P., 2006. Hf isotopic compositions of the standard zircons and baddeleyites used in U-Pb geochronology. Chem. Geol. 234, 105–126.
Xie, J.C., Zhu, D.C., Dong, G.C., Zhao, Z.D., Wang, Q., Mo, X.X., 2016. Linking the Tengchong Terrane in SW Yunnan with the Lhasa Terrane in southern Tibet through magmatic correlation. Gondwana Res. 39, 217–229.
Xu, Y.G., Yang, Q.J., Lan, J.B., Luo, Z.Y., Huang, X.L., Shi, Y.R., Xie, L.W., 2012. Temporal-spatial distribution and tectonic implications of the batholiths in the Gaoligong-Tengliang-Yingjiang area, western Yunnan: constraints from zircon U-Pb ages and Hf isotopes. J. Asian Earth Sci. 53, 151–175.
Yang, J.S., Xu, Z.Q., Duan, X.D., Li, J., Xiong, F.H., Liu, Z., Cai, Z.H., Li, H.Q., 2012. Discovery of a Jurassic SSZ ophiolite in the Myitkyina region of Myanmar. Acta Petrol. Sin. 28, 1710–1730 (in Chinese with English abstract).
Yin, A., Harrison, T.M., 2000. Geologic evolution of the Himalayan-Tibetan orogen. Annu. Rev. Earth Planet. Sci. 28, 211–280.
YNBGMR, 1990. Regional Geology of the Yunnan Province. Geological Publishing House, Beijing.
Zhao, S.W., Lai, S.C., Qin, J.F., Zhu, R.Z., 2016. Tectono-magmatic evolution of the Gaoligong belt, southeastern margin of the Tibetan plateau: constraints from granitic gneisses and granitoid intrusions. Gondwana Res. 35, 238–256.
Zhao, S.W., Lai, S.C., Gao, L., Qin, J.F., Zhu, R.Z., 2017a. Evolution of the Proto-Tethys in the Baoshan block along the East Gondwana margin: constraints from early Palaeozoic magmatism. Int. Geol. Rev. 59, 1–15.
Zhao, S.W., Lai, S.C., Qin, J.F., Zhu, R.Z., Wang, J.B., 2017c. Geochemical and geochronological characteristics of late Cretaceous to Early Paleocene granitoids in the Tengchong Block, Southwestern China: implications for crustal anatexis and thickness variations along the eastern Neo-Tethys subduction zone. Tectonophysics 694, 87–100.
Zhu, B.Q., Mao, C.X., Lugmair, G.W., Macdougall, J.D., 1983. Isotopic and geochemical evidence for the origin of Plio-Pleistocene volcanic rocks near the Indo-Eurasian collisional margin at Tengchong, China. Earth Planet. Sci. Lett. 65 (2), 263–275.
Zhu, D.C., Mo, X.X., Niu, Y.L., Zhao, Z.D., Wang, L.Q., Liu, Y.S., Wu, F.Y., 2009. Geochemical investigation of Early Cretaceous igneous rocks along an east-west traverse throughout the central Lhasa Terrane, Tibet. Chem. Geol. 268, 298–312.
Zhu, D.C., Zhao, Z.D., Niu, Y.L., Mo, X.X., Chung, S.L., Hou, Z.Q., Wang, L.Q., Wu, F.Y., 2011. The Lhasa Terrane: record of a microcontinent and its histories of drift and growth. Earth Planet. Sci. Lett. 301, 241–255.
Zhu, R.Z., Lai, S.C., Qin, J.F., Zhao, S.W., 2015. Early Cretaceous highly fractionated I-type granites from the northern Tengchong block, western Yunnan, SW China: petrogenesis and tectonic implications. J. Asian Earth Sci. 100, 145–163.
Zhu, R.Z., Lai, S.C., Qin, J.F., Zhao, S.W., Wang, J.B., 2017a. Late Early-Cretaceous quartz diorite-granodiorite-monzogranite association from the Gaoligong belt, southeastern Tibet Plateau: chemical variations and geodynamic implications. Lithos 288, 311–325.
Zhu, R.Z., Lai, S.C., Santosh, M., Qin, J.F., Zhao, S.W., 2017b. Early Cretaceous Na-rich granitoids and their enclaves in the Tengchong Block, SW China: magmatism in relation to subduction of the Bangong-Nujiang Tethys ocean. Lithos 286, 175–190.